Lattice Boltzmann Methods for Computational Fluid Dynamics

Li-Shi Luo

National Institute of Aerospace
144 Research Drive
Hampton, Virginia 23666, USA

Email: luo@nianet.org
URL: http://research.nianet.org/~luo

August 7 – 12, 2003
Institut für Computeranwendungen im Bauingenieurwesen (CAB)
Technischen Universität Braunschweig
Pockelsstraße 3, 38106 Braunschweig, Germany

Contents

List of Figures

List of Tables

Abstract

The Lecture Notes are used for the a short course on the theory and applications of the lattice Boltzmann methods for computational fluid dynamics taugh by the author at Institut für Computeranwendungen im Bauingenieurwesen (CAB), Technischen Universität Braunschweig, during August 7 – 12, 2003. The lectures cover the basic theory of the lattice Boltzmann equation and its applications to hydrodynamics. Lecture One briefly reviews the history of the lattice gas automata and the lattice Boltzmann equation and their connections. Lecture Two provides an *a priori* derivation of the lattice Boltzmann equation, which connects the lattice Boltzmann equation to the continuous Boltzmann equation and demonstrates that the lattice Boltzmann equation is indeed a special finite difference form of the Boltzmann equation. Lecture Two also includes the derivation of the lattice Boltzmann model for nonideal gases from the Enskog equation for dense gases. Lecture Three studies the generalized lattice Boltzmann equation with multiple relaxation times. A summary is provided at the end of each Lecture. Lecture Four discusses the fluid-solid boundary conditions in the lattice Boltzmann methods. Applications of the lattice Boltzmann mehod to particulate suspensions, turbulence flows, and other flows are also shown. An Epilogue on the rationale of the lattice Boltzmann method is given. Some key references in the literature is also provided.

Lecture 1

From Lattice Gas Automata to Lattice Boltzmann Equation — A Historic Review

1.1 Lattice Gas Automata

1.1.1 evolution of lattice gas automata

The lattice gas automaton (LGA) model proposed by Frisch, Hasslacher, and Pomeau [14], and Wolfram [65] evolves on a two-dimensional triangular lattice space. The particles have momenta that allow them to move from one site on the lattice to another in discrete time steps. A particular lattice site is occupied by either no particle or one particle with a particular momentum pointing to a nearest neighboring site. Therefore, at the most a lattice site can be simultaneously occupied by six particles, hence this model is called the six-velocity model or FHP-I model. The evolution of the LGA model consists of two steps: collision and advection. The collision process is partially described in Fig. 1.1. For example, two particles colliding with opposite momenta will rotate their momenta 60° clockwise or counter-clockwise with equal probability. In Fig. 1.1, we do not list those configurations which can be obtained by rotational transformation, and which are invariant under the collision process. The particle number, the momentum, and the energy are conserved in the collision process locally and exactly. (Because the FHP-I model has only one speed, the energy is no longer an independent variable, it is equivalent to the particle number. However, for multi-speed models, the energy is an independent variable.)

The evolution of the lattice gas automata is very simple. The collision step only involves local information, and the advection step is uniform. Both collision and advection processes at each lattice site can be executed synchronously. The evolution equation of the lattice gas automata can be written as

$$n_\alpha(\boldsymbol{x}_i + \boldsymbol{e}_\alpha,\, t+1) = n_\alpha(\boldsymbol{x}_i,\, t) + C_\alpha(\{n_\beta\})\,, \tag{1.1}$$

where $n_\alpha(\boldsymbol{x}_i,\, t)$ is the (Boolean) particle number of particles with velocity $\boldsymbol{e}_\alpha$, $n_\alpha \in \{0,\, 1\}$; the subscript α and β denote discrete velocities, $\alpha,\ \beta \in \{1,\, 2,\, \cdots,\, b\}$ as illustrated in Fig. 1.1, where b is the total number of the discrete velocities in the set $\{\boldsymbol{e}_\alpha | \alpha = 1,\, 2,\, \ldots,\, b\}$; and the discrete velocities in the FHP-I model are given by

$$\boldsymbol{e}_\alpha \equiv (\cos[(\alpha-1)\pi/3],\, \sin[(\alpha-1)\pi/3])\,, \qquad \alpha = 1,\ 2,\ \ldots,\, 6, \tag{1.2}$$

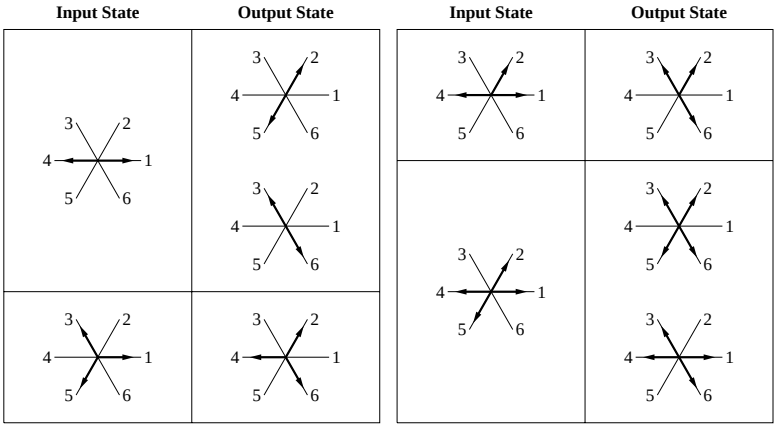

Figure 1.1: Collisions of FHP LGA model. Note that the figure does not included those collisions that can be obtained by applying rotations of multiple $\pi/3$ to input and output states simultaneously.

and $C_\alpha(n)$ is the collision operator, and $C_\alpha \in \{-1, 0, 1\}$ for any Boolean LGA models. The local hydrodynamic quantities, such as density ρ and momentum $\rho\boldsymbol{u}$ are related to $\{n_\alpha\}$ by

$$\rho(\boldsymbol{x}_i, t) = m \sum_\alpha n_\alpha(\boldsymbol{x}_i, t)\,, \tag{1.3a}$$

$$\rho\boldsymbol{u}(\boldsymbol{x}_i, t) = m \sum_\alpha \boldsymbol{e}_\alpha n_\alpha(\boldsymbol{x}_i, t)\,. \tag{1.3b}$$

Fig. 1.2 illustrates the evolution of the system in one time step from t to $t+\delta_t$. In this figure, solid and hollow arrows represent particles with corresponding velocity at time t and $t+\delta_t$, respectively. The system evolves by iteration of the collision and advection processes. Evolution from t (solid arrows) to $t+1$ (hollow arrows):

1.1.2 collision operator

The collision operator is constructed such that the local conservation laws of mass, momentum, and energy are *exactly* preserved, *i.e.*,

$$\sum_\alpha C_\alpha = 0\,, \tag{1.4a}$$

$$\sum_\alpha \boldsymbol{e}_\alpha C_\alpha = 0\,, \tag{1.4b}$$

$$\sum_\alpha \boldsymbol{e}_\alpha^2 C_\alpha = 0\,. \tag{1.4c}$$

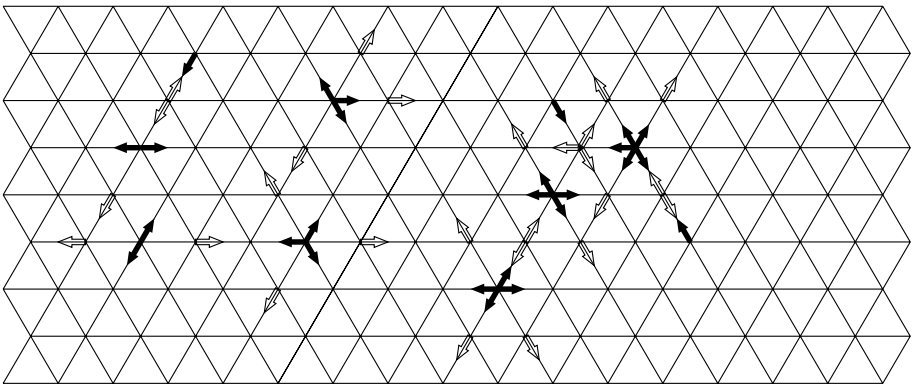

Figure 1.2: Evolution of FHP LGA model. Solid and hollow arrows represent particles with velocities corresponding to times t and $t+1$, respectively. That is, the hollow arrows are the final configurations of the initial configurations of solid arrows after one cycle of collision and advection.

For the FHP model, the collision operator can be written in general as the following

$$\begin{aligned} C_\alpha(\{n_\alpha(\boldsymbol{x},\, t)\}) &= \sum_{\boldsymbol{s},\,\boldsymbol{s}'} (s'_\alpha - s_\alpha)\, \xi_{\boldsymbol{s}\boldsymbol{s}'} \prod_{\sigma=1}^{b} n_\sigma^{s_\sigma} (1-n_\sigma)^{(1-s_\sigma)} \\ &= \sum_{\boldsymbol{s},\,\boldsymbol{s}'} (s'_\alpha - s_\alpha)\, \xi_{\boldsymbol{s}\boldsymbol{s}'} \prod_{\sigma=1}^{b} \delta_{n_\sigma s_\sigma} \end{aligned} \tag{1.5}$$

where $\boldsymbol{s} \equiv \{s_1,\, s_2,\, \ldots,\, s_b\}$ and $\boldsymbol{s}' \equiv \{s'_1,\, s'_2,\, \ldots,\, s'_b\}$ are possible pre-collision and post-collision Boolean state, respectively. The Boolean random number $\xi_{\boldsymbol{s}\boldsymbol{s}'}$ must satisfy the following conditions (normalization, semi-detailed balance, and isotropy under the discrete symmetry rotational group $\mathcal{G}$):

$$\sum_{\boldsymbol{s}'} \xi_{\boldsymbol{s}\boldsymbol{s}'} = 1\,, \qquad \forall\, \boldsymbol{s}\,, \tag{1.6a}$$

$$\sum_{\boldsymbol{s}} \xi_{\boldsymbol{s}\boldsymbol{s}'} = 1\,, \qquad \forall\, \boldsymbol{s}'\,, \tag{1.6b}$$

$$\xi_{g(\boldsymbol{s})g(\boldsymbol{s}')} = \xi_{\boldsymbol{s}\boldsymbol{s}'}\,, \qquad \forall\, g \in \mathcal{G}\,, \text{ and } \forall\, \boldsymbol{s},\ \boldsymbol{s}', \tag{1.6c}$$

and the conservation laws of mass, momentum, and energy:

$$\sum_\alpha (s_\alpha - s'_\alpha)\langle \xi_{\boldsymbol{s}\boldsymbol{s}'} \rangle = 0\,, \tag{1.7a}$$

$$\sum_\alpha (s_\alpha - s'_\alpha)\boldsymbol{e}_\alpha \langle \xi_{\boldsymbol{s}\boldsymbol{s}'} \rangle = 0\,, \tag{1.7b}$$

$$\sum_\alpha (s_\alpha - s'_\alpha)\boldsymbol{e}_\alpha^2 \langle \xi_{\boldsymbol{s}\boldsymbol{s}'} \rangle = 0\,. \tag{1.7c}$$

Input State	Output State
001001	010010 100100
010101	101010
001011	100110
011011	110110 101101

Table 1.1: Collision table for the FHP-I six-velocity model.

For example, the two-body collision term in the six-velocity FHP model is given by

$$\begin{aligned} C_\alpha^{(2)} &= +\xi_R^{(2)}\, n_{\alpha+1} n_{\alpha+4} \bar{n}_\alpha \bar{n}_{\alpha+2} \bar{n}_{\alpha+3} \bar{n}_{\alpha+5} \\ &\quad +\xi_L^{(2)}\, n_{\alpha+2} n_{\alpha+5} \bar{n}_\alpha \bar{n}_{\alpha+1} \bar{n}_{\alpha+3} \bar{n}_{\alpha+4} \\ &\quad -[\xi_R^{(2)} + \xi_L^{(2)}]\, n_\alpha n_{\alpha+3} \bar{n}_{\alpha+1} \bar{n}_{\alpha+2} \bar{n}_{\alpha+4} \bar{n}_{\alpha+5}\ , \end{aligned} \tag{1.8}$$

where $\bar{n}_\alpha \equiv (1 - n_\alpha)$ is the Boolean complement of n_α $\xi_R^{(2)}$ and $\xi_L^{(2)}$ the Boolean random numbers which determine a head-on two-body collision to rotate 60° clockwise (L) or counter-clockwise (R), as illustrated in Fig. 1.1, and they must satisfy the isotropic condition: $\langle \xi_R^{(2)} \rangle = \langle \xi_L^{(2)} \rangle$, and

In practice, the collision can be implemented with various algorithms. One can either use logical operations, or by table-lookup. The collision rules shown in Fig. 1.1 can also be represented by a collision table, as shown by Table 1.1. In Table 1.1, each bit in a binary number represents a particle number n_α, $\alpha = 1, 2, \ldots, 6$, from right to left. The limitation of table lookup is the size of the table, which is 2^b, where b is the number of discrete velocities in the model. Both logic operations and table lookup can be extremely fast on digital computers, and especially so on dedicated computers [60].

1.2 Chapman-Enskog Analysis

The Chapman-Enskog analysis is a procedure to solve the Boltzmann equation by means of (asymptotic) perturbation technique [4]. Through the solution of the Boltzmann equation, the hydrodynamic equations and transport coefficients can be derived from macroscopic dynamics. Based on dimensional analysis, a dimensionless parameter ε can be introduced in the collision term in the Boltzmann equation:

$$\partial_t f + \boldsymbol{\xi} \cdot \boldsymbol{\nabla} f = \frac{1}{\varepsilon} C(f, f), \qquad \varepsilon \equiv K_n = \frac{l}{L}\,, \tag{1.9}$$

where the perturbation parameter ε is the Knudsen number, which is the ratio between microscopic and macroscopic characteristic lengths, l and L. The normal solution of the Boltzmann equation satisfies the following *ansatz*:

$$f(\boldsymbol{x},\, \boldsymbol{\xi},\, t) = f(\boldsymbol{x},\, \boldsymbol{\xi};\, \rho,\, \boldsymbol{u},\, T)\,. \tag{1.10}$$

That is, the time dependence of the normal solution is through its dependence on the local hydrodynamic (conserved) moments ρ, $\boldsymbol{u}$, and T. The distribution function $f(\boldsymbol{x},\, \boldsymbol{\xi},\, t)$ can be expanded in terms of ε

$$f = \sum_{n=0}^{\infty} \varepsilon^n f^{(n)}, \tag{1.11}$$

with the constraints

$$\int d\boldsymbol{\xi} f^{(0)} \begin{bmatrix} 1 \\ \boldsymbol{\xi} \\ (\boldsymbol{\xi}-\boldsymbol{u})^2 \end{bmatrix} = \rho \begin{bmatrix} 1 \\ \boldsymbol{u} \\ D\theta \end{bmatrix}, \tag{1.12}$$

$$\int d\boldsymbol{\xi} f^{(n)} \begin{bmatrix} 1 \\ \boldsymbol{\xi} \\ (\boldsymbol{\xi}-\boldsymbol{u})^2 \end{bmatrix} = 0\,, \qquad n \geq 1\,, \tag{1.13}$$

i.e., the higher order, non-equilibrium parts of f do not contribute to the hydrodynamic (conserved) moments. However they do contribute to the gradients of the hydrodynamic moments. The collision term can also be expanded in terms of ε

$$C(f,\, f) = \sum_{n=0}^{\infty} \varepsilon^n C^{(n)}\,, \qquad C^{(n)} = \sum_{k+l=n} C(f^{(k)}, f^{(l)})\,. \tag{1.14}$$

The normal solution can be obtained by solving the equations successively in the order of ε:

$$O(\varepsilon^{-1}): \qquad C(f^{(0)},\, f^{(0)}) = 0, \tag{1.15a}$$

$$O(\varepsilon^{0}): \qquad \partial_t f^{(0)} + \boldsymbol{\xi}\cdot\boldsymbol{\nabla} f^{(0)} = 2C(f^{(0)},\, f^{(1)}). \tag{1.15b}$$

The $O(\varepsilon^{-1})$ equation yields the Maxwellian equilibrium distribution function:

$$f^{(0)} = \frac{\rho}{(2\pi\theta)^{D/2}} \exp\left[-\frac{(\boldsymbol{\xi}-\boldsymbol{u})^2}{2\theta}\right]. \tag{1.16}$$

In general it is laborious to obtain the first order solution $f^{(1)}$ [4]. However, for the Boltzmann equation with Bhatnagar-Gross-Krook approximation [1],

$$\partial_t f + \boldsymbol{\xi}\cdot\boldsymbol{\nabla} f = -\frac{1}{\lambda}[f - f^{(0)}]\,, \tag{1.17}$$

the first order solution is easy to obtain:

$$f^{(1)} = -\lambda(\partial_t f^{(0)} + \boldsymbol{\xi}\cdot\boldsymbol{\nabla} f^{(0)})\,, \tag{1.18}$$

The hydrodynamic equations are obtained by evaluating the moments of the Boltzmann equation with the normal solutions:

$$\int d\boldsymbol{\xi}\,(\partial_t f + \boldsymbol{\xi}\cdot\boldsymbol{\nabla} f)\begin{bmatrix} 1 \\ \boldsymbol{\xi} \\ \frac{1}{2}(\boldsymbol{\xi}-\boldsymbol{u})^2 \end{bmatrix} = 0\,. \tag{1.19}$$

The above equation leads to the Euler equations for $f = f^{(0)}$, and to the Navier-Stokes equations for $f = f^{(0)} + f^{(1)}$.

1.3 Lattice Gas Automata Hydrodynamics

The ensemble average of the LGA evolution equation 1.1 with the assumption of random phase leads to the following equation [15]:

$$f_\alpha(\boldsymbol{x}_i + \boldsymbol{e}_\alpha,\, t+1) = f_\alpha(\boldsymbol{x}_i,\, t) + \Omega_\alpha(f)\,, \tag{1.20}$$

where $f_\alpha(\boldsymbol{x}_i,\, t)$ is the single particle distribution function with discrete velocity $\boldsymbol{e}_\alpha$, $f_\alpha = \langle n_\alpha\rangle \in [0,\, 1]$. The lattice Boltzmann collision operator $\Omega_\alpha(f) = \langle C_\alpha(n)\rangle \in [-1,\, 1]$ is given by:

$$\Omega_\alpha(f) = \sum_{\boldsymbol{s},\,\boldsymbol{s}'}(s'_\alpha - s_\alpha)\,\langle\xi_{\boldsymbol{s}\boldsymbol{s}'}\rangle\prod_{\sigma=1}^{b} f_\sigma^{s_\sigma}(1-f_\sigma)^{(1-s_\sigma)}\,, \tag{1.21}$$

where $C_\alpha(n)$ is the LGA collision operator, and the random phase (molecular chaos) assumption is used to obtain $\Omega_\alpha(f)$:

$$\langle f_\alpha f_\beta\cdots f_\gamma\rangle = \langle f_\alpha\rangle\langle f_\beta\rangle\cdots\langle f_\gamma\rangle \tag{1.22}$$

The local hydrodynamic moments are computed from $\{f_\alpha\}$ as the following:

$$\rho(\boldsymbol{x}_i,\, t) = \sum_\alpha f_\alpha(\boldsymbol{x}_i,\, t)\,, \tag{1.23a}$$

$$\rho\boldsymbol{u}(\boldsymbol{x}_i,\, t) = \sum_\alpha \boldsymbol{e}_\alpha f_\alpha(\boldsymbol{x}_i,\, t)\,. \tag{1.23b}$$

Due to the Boolean nature of the lattice-gas automata, the equilibrium distribution, which is the solution of $\Omega_\alpha(f) = 0$, is a Fermi-Dirac distribution:

$$f_\alpha^{(0)} = \frac{1}{1+\exp(a+\boldsymbol{b}\cdot\boldsymbol{e}_\alpha)}\,, \tag{1.24}$$

where a and $\boldsymbol{b}$ are functions of the conserved moments and cannot be obtained analytically in general. Usually, a and $\boldsymbol{b}$ are obtained perturbatively as Taylor series of ρ and $\boldsymbol{u}$ in the limit of low Mach number (small $\boldsymbol{u}$).

By applying the Chapman-Enskog analysis in the hydrodynamic limit (long wave-length and low frequency) to the lattice Boltzmann equation (1.20), the following macroscopic equation can be derived from the Frisch-Hasslacher-Pomeau (FHP) lattice-gas automaton model [14, 65, 15] in the low March number limit:

$$\partial_t(\rho\boldsymbol{u}) + \boldsymbol{\nabla}\cdot[g(\rho)\rho\boldsymbol{u}\boldsymbol{u}] = -\boldsymbol{\nabla}P + \nu\nabla^2(\rho\boldsymbol{u}) + \eta\boldsymbol{\nabla}\boldsymbol{\nabla}\cdot(\rho\boldsymbol{u}). \tag{1.25}$$

The FHP-I (six-velocity) lattice-gas model have some obvious shortcomings:

- The LGA simulations are intrinsically noisy due to large fluctuation of particle number n_α. A spatial or temporal average is required to obtain smooth measurements;
- The LGA models are lack of Galilean invariance because the velocity space is discrete and finite. This is reflected by the fact that $g(\rho) \neq 1$ in the LGA hydrodynamic equation;
- The viscosity ν of the LGA models are determined by their collision mechanisms. It is difficult to increase the Reynolds number Re due to the lower bound of ν;
- The equation of state (for the FHP-I six-velocity model)

$$P = c_s^2\rho\left[1 - g(\rho)\,\frac{u^2}{c^2}\right] \tag{1.26}$$

  is unphysical because its dependence on u^2.
- There exist (unphysical) spurious conserved quantities due to the simplicity of spatial-temporal dynamics of the LGA systems.

Much of research effort has been to overcome the artifacts of the lattice gas automata. There are two approaches to remedy the shortcomings of the FHP-I lattice-gas automata. One is to construct more complicate lattice gas model with more discrete velocities. The other is to use the lattice Boltzmann equation.

1.4 Lattice Boltzmann Equation

Historically, the lattice Boltzmann equation is directly obtained from the lattice gas automata by taking ensemble average of Eq. (1.1) [48]. However, such lattice Boltzmann scheme is difficult to be generalized in three-dimensions, and it is computationally inefficient due to the cumbersome collision operator.

To improve the computational efficiency, one can use linearized collision operator [30]. The collision operator linearized about the equilibrium is given by

$$\mathcal{L}_{\alpha\beta} = \left.\frac{\partial \Omega_\beta}{\partial f_\alpha}\right|_{f=f^{(0)}} [f_\alpha - f_\alpha^{(0)}] \,. \tag{1.27}$$

With the linearized collision operator, the LBE computation is greatly simplified. The collision operator becomes a $b \times b$ matrix of constant matrix elements.

1.5 Lattice BGK Model

The linearized lattice Boltzmann equation can be further simplified by using the Bhatnagar-Gross-Krook approximation of single relaxation time [1]. Thus the collision process in the lattice BGK model [5, 55] is characterized by a relaxation time τ:

$$\Omega_\alpha(f) = -\frac{1}{\tau}[f_\alpha - f_\alpha^{(\mathrm{eq})}] \,. \tag{1.28}$$

The equilibrium distribution function is generally in the form of

$$f_\alpha^{(\mathrm{eq})} \;=\; w_\alpha \rho \left[1 + A\,(\boldsymbol{e}_\alpha \cdot \boldsymbol{u}) + B\,(\boldsymbol{e}_\alpha \cdot \boldsymbol{u})^2 + C\,\boldsymbol{u}^2\right] \,, \tag{1.29}$$

where w_α, A, B, and C are determined by conservation laws. The lattice BGK model [55, 5] is described by the following equation

$$f_\alpha(\boldsymbol{x}_i + \boldsymbol{e}_\alpha,\, t+1) = f_\alpha(\boldsymbol{x}_i,\, t) - \frac{1}{\tau}\left[f_\alpha(\boldsymbol{x}_i,\, t) - f_\alpha^{(\mathrm{eq})}(\boldsymbol{x}_i,\, t)\right] \,. \tag{1.30}$$

1.6 LBE Hydrodynamics

In the limits of K_n, δ_x, $\delta_t \to 0$, the Navier-Stokes equation can be derived from the lattice BGK equation:

$$\rho\, \partial_t \boldsymbol{u} + \rho\, \boldsymbol{u} \nabla{\cdot}\boldsymbol{u} = -\nabla P + \rho\, \nu \nabla^2 \boldsymbol{u} \,, \tag{1.31}$$

with the isothermal equation of state and the viscosity given by

$$P = c_s^2\, \rho \,, \tag{1.32a}$$

$$\nu = c_s^2 \left(\tau - \frac{1}{2}\right) \,, \tag{1.32b}$$

where $c_s \sim \sqrt{k_B T/m} = \sqrt{\theta}$ is the sound speed, depending on the discrete velocity set. For the FHP six-velocity model on a triangular lattice in two dimensions, $c_s = 1/\sqrt{2}$, and for the nine-velocity model on a square lattice n two dimensions, $c_s = 1/\sqrt{3}$.

Obviously, the lattice Boltzmann equation overcomes some the shortcomings of the lattice gas automata. First, the severe fluctuation is eliminated. Secondly, the viscosity is easy to adjust. Thirdly, Galilean invariance is restored up to a certain order in wave number k. And the equation of state has no unphysical dependence on u^2. However, the lattice Boltzmann equation cannot completely eliminate the spurious invariant quantities. In addition, the roundoff error causes instability in the lattice Boltzmann equation.

1.7 Summary

The lattice-gas automata have the following features:

- Mimicking (simplified) molecular dynamics of structureless particles;
- Exactly preserving conservation laws;
- Processing basic symmetries to simulate hydrodynamics;
- Including spurious conserved quantities due to simplicity of spatial-temporal dynamics;
- Large fluctuations is intrinsic to the system;
- LGA computation is Boolean in nature (integer or logic or table-lookup algorithms).

In contrast, the lattice Boltzmann equation has the following features:

- Simulate hydrodynamics based on a drastically simplified Boltzmann equation with a small set of discrete velocities;
- Overcoming some defects of the lattice-gas automata, such as large fluctuations, inflexibility to adjust the viscosity, non-Galilean invariant, and unphysical equation of state.
- Better numerical efficiency in compared with the lattice gas automata under certain conditions.

In conclusion, the LGA and LBE methods can simulate hydrodynamics.

Lecture 2

Mathematical Derivation of the Lattice Boltzmann Models

2.1 Integral Solution of the Boltzmann Equation

For the sake of simplicity without losing generality, we study the continuous Boltzmann equation with Bhatnagar-Gross-Krook (BGK) approximation [1]:

$$\partial_t f + \boldsymbol{\xi}\cdot\nabla f = -\frac{1}{\lambda}[f - f^{(0)}], \qquad f \equiv f(\boldsymbol{x},\, \boldsymbol{\xi},\, t)\,, \tag{2.1}$$

where $f^{(0)}$ is the Boltzmann-Maxwellian equilibrium distribution function:

$$f^{(0)} = \rho\,(2\pi\theta)^{-D/2}\,\exp\left[-\frac{(\boldsymbol{\xi}-\boldsymbol{u})^2}{2\theta}\right], \tag{2.2}$$

where $\theta = k_B T/m$, k_B, T, and m are the Boltzmann constant, temperature, and particle mass, respectively. The macroscopic quantities are the hydrodynamic moments of f or $f^{(0)}$:

$$\rho = \int f d\boldsymbol{\xi} = \int f^{(0)} d\boldsymbol{\xi}\,, \tag{2.3a}$$

$$\rho\boldsymbol{u} = \int \boldsymbol{\xi} f d\boldsymbol{\xi} = \int \boldsymbol{\xi} f^{(0)} d\boldsymbol{\xi}\,, \tag{2.3b}$$

$$\frac{D}{2}\rho\theta = \frac{1}{2}\int (\boldsymbol{\xi}-\boldsymbol{u})^2 f d\boldsymbol{\xi} = \frac{1}{2}\int (\boldsymbol{\xi}-\boldsymbol{u})^2 f^{(0)} d\boldsymbol{\xi}\,. \tag{2.3c}$$

Rewrite the Boltzmann BGK Equation in the form of ODE:

$$D_t f + \frac{1}{\lambda} f = \frac{1}{\lambda} f^{(0)}\,, \qquad D_t \equiv \partial_t + \boldsymbol{\xi}\cdot\nabla\,, \tag{2.4}$$

and integrate Eq. (2.4) over a time step δ_t along characteristics, we have:

$$\begin{aligned} f(\boldsymbol{x}+\boldsymbol{\xi}\delta_t,\, \boldsymbol{\xi},\, t+\delta_t) &= e^{-\delta_t/\lambda}\, f(\boldsymbol{x},\, \boldsymbol{\xi},\, t) \\ &\quad + \frac{1}{\lambda} e^{-\delta_t/\lambda} \int_0^{\delta_t} e^{t'/\lambda}\, f^{(0)}(\boldsymbol{x}+\boldsymbol{\xi}t',\, \boldsymbol{\xi},\, t+t')\, dt'\,. \end{aligned} \tag{2.5}$$

By Taylor expansion, and with $\tau \equiv \lambda/\delta_t$, we obtain:

$$f(\boldsymbol{x}+\boldsymbol{\xi}\delta_t,\, \boldsymbol{\xi},\, t+\delta_t) - f(\boldsymbol{x},\, \boldsymbol{\xi},\, t) = -\frac{1}{\tau}[f(\boldsymbol{x},\, \boldsymbol{\xi},\, t) - f^{(0)}(\boldsymbol{x},\, \boldsymbol{\xi},\, t)] + \mathcal{O}(\delta_t^2)\,. \tag{2.6}$$

Note that a *finite-volume* scheme or higher-order schemes can also be formulated based upon the integral solution.

2.2 Passage to Lattice Boltzmann Equation

There are three necessary steps to obtain the lattice Boltzmann equation from Eq. (eqn:bgk-integral):

1. Low Mach number expansion of the equilibrium distribution function;
2. Discretization of velocity space $\boldsymbol{\xi}$ to obtain necessary and minimum number of discrete velocities $\{\boldsymbol{\xi}_\alpha\}$;
3. Discretization of $\boldsymbol{x}$ space according to $\{\boldsymbol{\xi}_\alpha\}$ and δ_t.

2.2.1 low Mach number expansion of the equilibrium distribution function

Low Mach number ($u \approx 0$) expansion of the equilibrium distribution function $f^{(0)}$ up to $O(u^2)$ is sufficient to derive the Navier-Stokes equations:

$$f^{(\mathrm{eq})} = \frac{\rho}{(2\pi\theta)^{D/2}} \exp\left[-\frac{\boldsymbol{\xi}^2}{2\theta}\right] \left\{1 + \frac{\boldsymbol{\xi}\cdot\boldsymbol{u}}{\theta} + \frac{(\boldsymbol{\xi}\cdot\boldsymbol{u})^2}{2\theta^2} - \frac{\boldsymbol{u}^2}{2\theta}\right\} + O(u^3)\,. \tag{2.7}$$

It should be noted that many defects of the lattice Boltzmann method are related to the above low Mach number expansion of the equilibrium function. However, this expansion is necessary to make the lattice Boltzmann method a *simple* and *explicit* scheme.

2.2.2 discretization and conservation laws

The conservation laws are preserved *exactly*, if the hydrodynamic moments (ρ, $\rho\boldsymbol{u}$, and $\rho\epsilon$) are evaluated *exactly*:

$$I = \int \boldsymbol{\xi}^m f^{(\mathrm{eq})} d\boldsymbol{\xi} = \int \exp(-\boldsymbol{\xi}^2/2\theta)\psi(\boldsymbol{\xi}) d\boldsymbol{\xi}, \tag{2.8}$$

where $0 \le m \le 3$, and $\psi(\boldsymbol{\xi})$ is a polynomial in $\boldsymbol{\xi}$. The above integral can be evaluated by quadrature:

$$I = \int \exp(-\boldsymbol{\xi}^2/2\theta)\psi(\boldsymbol{\xi}) d\boldsymbol{\xi} = \sum_j W_j \exp(-\boldsymbol{\xi}_j^2/2\theta)\psi(\boldsymbol{\xi}_j) \tag{2.9}$$

where $\boldsymbol{\xi}_j$ and W_j are the abscissas and the weights. Then

$$\rho = \sum_\alpha f_\alpha^{(\mathrm{eq})} = \sum_\alpha f_\alpha, \qquad \rho\boldsymbol{u} = \sum_\alpha \boldsymbol{\xi}_\alpha f_\alpha^{(\mathrm{eq})} = \sum_\alpha \boldsymbol{\xi}_\alpha f_\alpha, \tag{2.10}$$

where $f_\alpha \equiv f_\alpha(\boldsymbol{x}, t) \equiv W_\alpha f(\boldsymbol{x}, \boldsymbol{\xi}_\alpha, t)$, and $f_\alpha^{(\mathrm{eq})} \equiv W_\alpha f^{(\mathrm{eq})}(\boldsymbol{x}, \boldsymbol{\xi}_\alpha, t)$. The key message is that the quadrature must preserve the conservation laws *exactly*.

2.2.3 nine-velocity LBE model on a square lattice in two dimensions

In two-dimensional Cartesian (velocity) space, set

$$\psi(\boldsymbol{\xi}) = \xi_x^m \xi_y^n,$$

the integral of the moments can be given by

$$I = (\sqrt{2\theta})^{(m+n+2)} I_m I_n, \qquad I_m = \int_{-\infty}^{+\infty} e^{-\zeta^2} \zeta^m d\zeta, \tag{2.11}$$

where $\zeta = \xi_x/\sqrt{2\theta}$ or $\xi_y/\sqrt{2\theta}$. The second-order Hermite formula ($k = 2$) is the *optimal* choice to evaluate I_m for the purpose of deriving the nine-velocity model on a two-dimensional square lattice, *i.e.*,

$$I_m = \sum_{j=1}^{3} \omega_j \zeta_j^m.$$

Note that the above quadrature is *exact* up to $m = 5 = (2k+1)$. The three abscissas in momentum space (ζ_j) and the corresponding weights (ω_j) are:

$$\begin{array}{lll} \zeta_1 = -\sqrt{3/2}\,, & \zeta_2 = 0\,, & \zeta_3 = \sqrt{3/2}\,, \\ \omega_1 = \sqrt{\pi}/6\,, & \omega_2 = 2\sqrt{\pi}/3\,, & \omega_3 = \sqrt{\pi}/6\,. \end{array} \tag{2.12}$$

Then, the integral of moments becomes:

$$I = 2\theta \left[\omega_2^2 \psi(\mathbf{0}) + \sum_{\alpha=1}^{4} \omega_1 \omega_2 \psi(\boldsymbol{\xi}_\alpha) + \sum_{\alpha=5}^{8} \omega_1^2 \psi(\boldsymbol{\xi}_\alpha) \right], \tag{2.13}$$

where

$$\boldsymbol{\xi}_\alpha = \begin{cases} (0,\, 0) & \alpha = 0, \\ (\pm 1,\, 0)\sqrt{3\theta},\ (0,\, \pm 1)\sqrt{3\theta}, & \alpha = 1 - 4, \\ (\pm 1,\, \pm 1)\sqrt{3\theta}, & \alpha = 5 - 8. \end{cases} \tag{2.14}$$

Identifying $c \equiv \delta_x/\delta_t = \sqrt{3\theta}$, or $c_s^2 = \theta = c^2/3$,

$$W_\alpha = (2\pi\,\theta)\, \exp(\boldsymbol{\xi}_\alpha^2/2\theta)\, w_\alpha\,, \tag{2.15}$$

where δ_x is the lattice constant, then we have

$$\begin{aligned} f_\alpha^{(\mathrm{eq})}(\boldsymbol{x},\, t) &= W_\alpha\, f^{(\mathrm{eq})}(\boldsymbol{x},\, \boldsymbol{\xi}_\alpha,\, t) \\ &= w_\alpha\, \rho \left\{ 1 + \frac{3(\boldsymbol{e}_\alpha \cdot \boldsymbol{u})}{c^2} + \frac{9(\boldsymbol{e}_\alpha \cdot \boldsymbol{u})^2}{2c^4} - \frac{3\boldsymbol{u}^2}{2c^2} \right\}, \end{aligned} \tag{2.16}$$

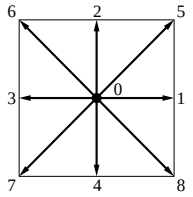

Figure 2.1: Discrete velocity set on a square lattice in two dimensions.

where weight coefficient w_α and discrete velocity $\boldsymbol{e}_\alpha$ are:

$$w_\alpha = \begin{cases} 4/9, \\ 1/9, \\ 1/36, \end{cases} \quad \boldsymbol{e}_\alpha = \boldsymbol{\xi}_\alpha = \begin{cases} (0,\,0), & \alpha = 0\,, \\ (\pm 1,\,0)\,c,\ (0,\,\pm 1)\,c, & \alpha = 1 - 4, \\ (\pm 1,\,\pm 1)\,c, & \alpha = 5 - 8. \end{cases} \tag{2.17}$$

With $\{\boldsymbol{e}_\alpha | \alpha = 0,\, 1,\, \ldots,\, 8\}$, a square lattice structure is constructed in the physical space, as shown in Fig. 2.1. (This model is also denoted as D2Q9 model.) Similarly, other LBE models in either two-dimensions (D2Q6 and D2Q7) or three-dimensions (D3Q27) can be derived [24].

2.3 Kinetic Theory for Dense Gases

2.3.1 Boltzmann's Theory for Rarefied Gases (1890')

The Boltzmann equation

$$\partial_t f + \boldsymbol{\xi} \cdot \boldsymbol{\nabla} f + \boldsymbol{a} \cdot \boldsymbol{\nabla}_\xi f = \int d\boldsymbol{\mu}_1 \, [f' f_1' - f f_1] \tag{2.18}$$

is valid in the *Boltzmann Gas Limit* (BGL):

$$\text{Particle Number} \qquad N \to \infty\,, \tag{2.19a}$$

$$\text{Interaction Range} \qquad r_0 \to 0\,, \tag{2.19b}$$

$$\text{Mean-Free-Path} \qquad l \sim (N r_0^2)^{-1} \to \text{Constant}\,, \tag{2.19c}$$

$$\text{Interaction Volume} \qquad N r_0^3 \to 0\,. \tag{2.19d}$$

Because of $N r_0^3 \to 0$, the Boltzmann equation can *only* retain the thermodynamics of *ideal* gases.

2.3.2 Enskog's Theory for Dense Gases (1917)

For hard spheres of radius r_0, the Boltzmann equation is modified for dense gases as follows (by Enskog):

$$\partial_t f + \boldsymbol{\xi} \cdot \boldsymbol{\nabla} f + \boldsymbol{a} \cdot \boldsymbol{\nabla}_\xi f = J\,, \tag{2.20}$$

where $\boldsymbol{a}$ is the acceleration due to external field, and J is the Enskog collision term

$$J = \int d\boldsymbol{\mu}_1 \left[g(\boldsymbol{x} + r_0\hat{\boldsymbol{r}}) f' f_1'(\boldsymbol{x} + 2r_0\hat{\boldsymbol{r}}) - g(\boldsymbol{x} - r_0\hat{\boldsymbol{r}}) f f_1(\boldsymbol{x} - 2r_0\hat{\boldsymbol{r}}) \right], \tag{2.21}$$

g is the radial distribution function, $\hat{\boldsymbol{r}}$ is the unit vector in the direction from the center of the second particle of $f(\boldsymbol{x},\, \boldsymbol{\xi}_1)$ to the center of the first particle of $f(\boldsymbol{x},\, \boldsymbol{\xi})$ at the instant of contact during a collision, and $\boldsymbol{\mu}_1$ is the collisional space of the second particle of $f(\boldsymbol{x},\, \boldsymbol{\xi}_1)$. The Enskog collision term J can be expanded as a Taylor series in space:

$$\begin{aligned}
J &= J^{(0)} + J^{(1)} + J^{(2)} + \cdots, && \text{(2.22a)} \\
J^{(0)} &= g \int d\boldsymbol{\mu}_1 [f' f_1' - f f_1], && \text{(2.22b)} \\
J^{(1)} &= r_0 \int d\boldsymbol{\mu}_1 \hat{\boldsymbol{r}} \cdot \boldsymbol{\nabla} g [f' f_1' + f f_1], && \text{(2.22c)} \\
J^{(2)} &= 2r_0 g \int d\boldsymbol{\mu}_1 \hat{\boldsymbol{r}} \cdot [f' \boldsymbol{\nabla} f_1' + f \boldsymbol{\nabla} f_1]. && \text{(2.22d)}
\end{aligned}$$

It is only necessary to retain terms up to the first order gradient.

The essence of Enskog's theory is to explicitly consider the volume exclusion effect in real gases consisting particles of finite sizes. The collision is non-local for particles of finite sizes. One ramification of the non-local collision is that the conservation laws only hold globally, but not locally. It should be noted that, similar to the Boltzmann equation, the Enskog equation has an H-Theorem and a consistent thermodynamics.

2.3.3 Enskog Closure of Two-Particle Distribution Function f_2

The essential assumption in Enskog's theory is the factorization of the two particle distribution function — the Enskog closure:

$$f_2(\boldsymbol{x}_1,\, \boldsymbol{\xi}_1,\, \boldsymbol{x}_2,\, \boldsymbol{\xi}_2,\, t) = g(|\boldsymbol{x}_1 - \boldsymbol{x}_2|) f_1(\boldsymbol{x}_1,\, \boldsymbol{\xi}_1,\, t) f_1(\boldsymbol{x}_2,\, \boldsymbol{\xi}_2,\, t), \tag{2.23}$$

where g is the radial distribution function (pairwise correlation). In contrast, the Boltzmann closure is

$$f_2(\boldsymbol{x}_1,\, \boldsymbol{\xi}_1,\, \boldsymbol{x}_2,\, \boldsymbol{\xi}_2,\, t) = f_1(\boldsymbol{x}_1,\, \boldsymbol{\xi}_1,\, t) f_1(\boldsymbol{x}_2,\, \boldsymbol{\xi}_2,\, t).$$

2.3.4 Non-Local Collision Terms in the Enskog Equation

With the approximation $f \approx f^{(0)}$, which is consistent with the Chapman-Enskog analysis, we have

$$J^{(1)} = -f^{(0)}\, b\, \rho\, \boldsymbol{\xi}_0 \cdot \boldsymbol{\nabla} g, \tag{2.24a}$$

$$
\begin{aligned}
J^{(2)} &= -f^{(0)}\, b\, \rho\, g \left[2\boldsymbol{\xi}_0 \cdot \boldsymbol{\nabla} \ln \rho + \frac{2}{(D+2)} \frac{\xi_{0i}\, \xi_{0j}\, \partial_i u_j}{\theta} \right. \\
&\quad + \left(\frac{1}{(D+2)} \frac{\boldsymbol{\xi}_0^2}{\theta} - 1 \right) \boldsymbol{\nabla} \cdot \boldsymbol{u} \\
&\quad \left. + \frac{1}{2} \left(\frac{D}{(D+2)} \frac{\boldsymbol{\xi}_0^2}{\theta} - 1 \right) \boldsymbol{\xi}_0 \cdot \boldsymbol{\nabla} \ln \theta \right] , \qquad (2.24b)
\end{aligned}
$$

where $f^{(0)}$ is the Maxwellian equilibrium distribution function given by

$$
f^{(0)}(\rho,\, \boldsymbol{u},\, \theta) = \rho (2\pi\theta)^{-D/2} \exp\left[-\frac{(\boldsymbol{\xi} - \boldsymbol{u})^2}{2\theta} \right] , \qquad (2.25)
$$

and $\boldsymbol{\xi}_0 = (\boldsymbol{\xi} - \boldsymbol{u})$ is the peculiar velocity, $\theta = k_B T/m$ is the normalized temperature, and $b = V_0/m = 4\pi r_0^3/3m$ is the second virial coefficient.

2.3.5 Normal Solutions of the Enskog Equation

The first and second order normal solution of the Enskog equation, obtained *via* Chapman-Enskog analysis, are:

$$
f^{(0)} = \rho\, (2\pi\theta)^{-D/2} \exp\left[-\frac{(\boldsymbol{\xi} - \boldsymbol{u})^2}{2\theta} \right] , \qquad (2.26)
$$

$$
\begin{aligned}
f^{(1)} = -f^{(0)} \frac{1}{g} \left[\left(1 + \frac{2}{(D+2)} b\rho g \right) \boldsymbol{A} \cdot \boldsymbol{\nabla} \ln \theta \right. \\
\left. + \left(1 + \frac{4}{D(D+2)} b\rho g \right) \mathsf{B}_{ij} \partial_i u_j \right] . \qquad (2.27)
\end{aligned}
$$

With $b = 0$ and $g = 1$, the solutions reduce to that of the Boltzmann equation.

Note that $\boldsymbol{\nabla}\rho$ does *not* appear in $f^{(1)}$, it appears in $f^{(2)}$ — the Burnett solution (1935). This is consistent with the dimensional analysis of the Navier-Stokes equation, $\boldsymbol{\nabla}\rho$ is in the order of $O(K_n^2)$, where K_n is the Knudsen number, which is also the small expansion parameter in the Chapman-Enskog analysis.

2.3.6 The Navier-Stokes Equations

The Navier-Stokes equations derived from the Enskog equation are

$$
\partial_t \rho + \boldsymbol{\nabla} \cdot (\rho \boldsymbol{u}) = 0 , \qquad (2.28a)
$$

$$
\partial_t \boldsymbol{u} + \boldsymbol{u} \cdot \boldsymbol{\nabla} \boldsymbol{u} = -\frac{1}{\rho} \boldsymbol{\nabla} \mathsf{P} + \boldsymbol{a} , \qquad (2.28b)
$$

$$
\partial_t \theta + \boldsymbol{u} \cdot \boldsymbol{\nabla} \theta = -\frac{1}{\rho} \boldsymbol{\nabla} \cdot \boldsymbol{q} - \frac{1}{\rho} \mathsf{P}_{ij} \partial_i u_j + \boldsymbol{a} \cdot \boldsymbol{u} , \qquad (2.28c)
$$

where

$$\mathsf{P}_{ij} = \int d\boldsymbol{\xi}\, \xi_{0i}\xi_{0j} f = [\rho\theta(1+b\rho g) - \eta_2 \boldsymbol{\nabla}\cdot \boldsymbol{u}]\, \delta_{ij} - \left[\frac{2}{g}\left(1+\frac{4}{D(D+2)} b\rho g\right)^2 \eta_1 + \frac{2D}{(D+2)}\eta_2\right] \mathsf{S}_{ij}\,, \tag{2.29a}$$

$$\mathsf{S}_{ij} = \frac{1}{2}[\partial_i u_j + \partial_j u_i] - \frac{1}{D}\boldsymbol{\nabla}\cdot \boldsymbol{u}\, \delta_{ij}\,, \tag{2.29b}$$

$$\boldsymbol{q} = \int d\boldsymbol{\xi} \frac{1}{2}\xi_0^2 \boldsymbol{\xi}_0 f = -\left[\frac{1}{g}(1+b\rho g)^2\kappa + \frac{D}{2}\eta_2\right] \boldsymbol{\nabla}\theta\,. \tag{2.29c}$$

2.3.7 Incompressible and Isothermal Fluids

Because for incompressible and isothermal fluids, $\boldsymbol{\nabla}\cdot\boldsymbol{u} = 0$ and $\boldsymbol{\nabla}\theta = 0$, therefore,

$$\begin{aligned} J^{(1)} + J^{(2)} &\approx -f^{(0)}\, b\rho\, (\boldsymbol{\xi} - \boldsymbol{u})\cdot[\boldsymbol{\nabla} g + g\boldsymbol{\nabla}\ln\rho^2] \\ &= -f^{(0)}\, b\rho\, g\, (\boldsymbol{\xi} - \boldsymbol{u})\cdot\boldsymbol{\nabla}\ln(\rho^2 g) = J'\,. \end{aligned} \tag{2.30}$$

The modified Boltzmann equation, with BGK approximation, is

$$\partial_t f + \boldsymbol{\xi}\cdot\boldsymbol{\nabla} f + \boldsymbol{a}\cdot\boldsymbol{\nabla}_\xi f = -\frac{g}{\lambda}[f - f^{(0)}] - f^{(0)}\, b\rho\, g\, (\boldsymbol{\xi} - \boldsymbol{u})\cdot\boldsymbol{\nabla}\ln(\rho^2 g)\,. \tag{2.31}$$

The equation of state derived from the above modified Boltzmann equation (obtained by computing the first moment of the non-local collision term) is

$$P = \rho\,\theta\,[1 + b\rho\, g]\,, \qquad g = g(b\rho)\,. \tag{2.32}$$

It should be noted that the non-ideal gas effects come from the non-local collision term, which is the manifestation of the volume exclusion effect, or other inter-particle interactions. It cannot be a result due to a body force.

2.4 Lattice Boltmzann Model for Dense Gases

2.4.1 Discretization of Continuous Enskog Equation

Similar to the previous Section, we can rewrite the Enskog BGK Equation in the form of ODE:

$$\frac{df}{dt} + \frac{g}{\lambda} f = \frac{g}{\lambda} f^{(0)} + J'\,, \qquad \frac{d}{dt} \equiv \frac{\partial}{\partial t} + \boldsymbol{\xi}\cdot\boldsymbol{\nabla} + \boldsymbol{a}\cdot\boldsymbol{\nabla}_\xi\,. \tag{2.33}$$

Integration of Eq. (2.33) over a time step δ_t along characteristic line leads to

$$\begin{aligned} f(\boldsymbol{x} + \boldsymbol{\xi}\delta_t + \frac{1}{2}\boldsymbol{a}\delta_t^2,\, \boldsymbol{\xi} + \boldsymbol{a}\delta_t,\, t + \delta_t) &= e^{-\delta_t g/\lambda}\, f(\boldsymbol{x},\, \boldsymbol{\xi},\, t) \\ + e^{-\delta_t g/\lambda} \int_0^{\delta_t} dt'\, e^{t' g/\lambda} \left[\frac{g}{\lambda} f^{(0)} + J'\right]_{(\boldsymbol{x} + \boldsymbol{\xi} t' + \frac{1}{2}\boldsymbol{a} t'^2,\, \boldsymbol{\xi} + \boldsymbol{a} t',\, t + t')}\,. \end{aligned} \tag{2.34}$$

By Taylor expansion, and with $\tau \equiv \lambda/\delta_t$, we obtain:

$$f(\boldsymbol{x}+\boldsymbol{\xi}\delta_t,\,\boldsymbol{\xi},\,t+\delta_t) - f(\boldsymbol{x},\,\boldsymbol{\xi},\,t) = -\frac{g}{\tau}[f(\boldsymbol{x},\,\boldsymbol{\xi},\,t) - f^{(0)}(\boldsymbol{x},\,\boldsymbol{\xi},\,t)] + \left[J' - \boldsymbol{a}\cdot\boldsymbol{\nabla}_\xi f\right]\,\delta_t + \mathcal{O}(\delta_t^2)\,. \tag{2.35}$$

This completes the temporal discretization. The discretization of phase space $(\boldsymbol{x},\,\boldsymbol{\xi})$ can be accomplished in the same manner as discussed in the previous Lecture. However, there are two extra terms needed to be dealt with here: the forcing term and the Enskog collision term.

2.4.2 The External Forcing

The forcing term must satisfy the following moment constraints:

$$\int d\boldsymbol{\xi}\,\boldsymbol{a}\cdot\boldsymbol{\nabla}_\xi f = 0\,, \tag{2.36a}$$

$$\int d\boldsymbol{\xi}\,\boldsymbol{\xi}\,\boldsymbol{a}\cdot\boldsymbol{\nabla}_\xi f = -\rho\,\boldsymbol{a}\,, \tag{2.36b}$$

$$\int d\boldsymbol{\xi}\,\xi_i\xi_j\,\boldsymbol{a}\cdot\boldsymbol{\nabla}_\xi f = -\rho\,(a_i u_j + a_j u_i)\,. \tag{2.36c}$$

Similar to the equilibrium, the forcing term is expanded in term of $\boldsymbol{u}$ as the following

$$\boldsymbol{a}\cdot\boldsymbol{\nabla}_\xi f = -\rho\,\exp(-\boldsymbol{\xi}^2/2\theta)\,\left[\frac{1}{\theta}(\boldsymbol{\xi}-\boldsymbol{u}) + \frac{(\boldsymbol{\xi}\cdot\boldsymbol{u})}{\theta^2}\,\boldsymbol{\xi}\right]\cdot\boldsymbol{a}\,. \tag{2.37}$$

Note that in the above expansion, only the terms up to the first order in $\boldsymbol{u}$ have been retained, because there is an overall factor of δ_t in the forcing term. If the second-order moment constraint Eq. (2.36) is ignored:

$$\boldsymbol{a}\cdot\boldsymbol{\nabla}_\xi f = -\rho\,\exp(-\boldsymbol{\xi}^2/2\theta)\,\frac{1}{\theta}\,\boldsymbol{\xi}\cdot\boldsymbol{a}\,. \tag{2.38}$$

2.4.3 The Lattice Boltzmann Model for Nonideal Gases

The LBE model for non-ideal gases derived from the Enskog equation for dense gases is given as the following:

$$f_\alpha(\boldsymbol{x}+\boldsymbol{e}_\alpha\delta_t,\,t+\delta_t) - f_\alpha(\boldsymbol{x},\,t) = -\frac{g}{\tau}[f_\alpha - f_\alpha^{(\mathrm{eq})}] + (J'_\alpha + F_\alpha)\,\delta_t \tag{2.39}$$

where

$$J'_\alpha = -f_\alpha^{(\mathrm{eq})} b\rho g\,(\boldsymbol{e}_\alpha - \boldsymbol{u})\cdot\boldsymbol{\nabla}\ln(\rho^2 g)\,, \tag{2.40a}$$

$$F_\alpha = w_\alpha\rho\left[\frac{3}{c^2}(\boldsymbol{e}_\alpha - \boldsymbol{u}) + \frac{9}{c^4}(\boldsymbol{e}_\alpha\cdot\boldsymbol{u})\boldsymbol{e}_\alpha\right]\cdot\boldsymbol{a}\,. \tag{2.40b}$$

The equation of state and the viscosity of the model are given by

$$P = \rho\theta[1 + b\rho g]\,, \tag{2.41a}$$

$$\nu = \frac{1}{3}\left(\frac{\tau}{g} - \frac{1}{2}\right) c\,\delta_x = \left(\frac{\tau}{g} - \frac{1}{3}\right)\theta\,\delta_t\,. \tag{2.41b}$$

Note that the viscosity depends on the radial distribution function g. This dependence of ν on g can be eliminated by setting the relaxation parameter to $1/\tau$. For hard-spheres, the radial distribution function is [4]

$$g = 1 + \frac{5}{8}b\rho + 0.2869(b\rho)^2 + \ldots\,.$$

2.5 Some Recent Progress

Once it is realized that the lattice Boltzmann equation is related to a partial differential equation, the Boltzmann equation, many numerical techniques used to solve PDEs can be immediately applied to solve the lattice Boltzmann equation.

First, one can abandon the regular lattice of the LBE method by decoupling the discretizations between space, time and momentum space, and using interpolation/extrapolation techniques [26, 27]. With the freedom of using interpolation/extrapolation techniques, both body-fitted mesh [22, 23] and grid refinement [13] can be implemented in the LBE method.

Secondly, one can devise implicit method [62] or multi-grid technique to solve the lattice Boltzmann equation for steady state calculations. These techniques can accelerate the computational speed by two orders of magnitude.

2.6 A Critical Review of Existing Lattice Boltzmann Models for Nonideal Gases

2.6.1 General ideas the LBE Models for Nonideal Gases (1990')

The usual practice to achieve nonideal gas effect by using a lattice Boltzmann model consists the following two tricks:

- Use of interaction potential, or "*brute force*";
- Creation of "*new*" and "*nonideal*" equilibrium distribution function.

That is, given a hydrodynamic equation with an (almost) arbitrary stress tensor Π:

$$\rho\partial_t \boldsymbol{u} + \rho\boldsymbol{u}\cdot\boldsymbol{\nabla}\boldsymbol{u} = \boldsymbol{\nabla}\Pi$$

Then, employ the following tricks:

$$\left.\begin{array}{l} \sum_\alpha \boldsymbol{e}_{\alpha,i}\boldsymbol{e}_{\alpha,j} f_\alpha^{(\mathrm{eq})} \\ \sum_\alpha \boldsymbol{e}_{\alpha,i}\boldsymbol{e}_{\alpha,j} F_\alpha \end{array}\right\} \Rightarrow \boldsymbol{\nabla}\Pi$$

2.6.2 Model with Interaction Potential

Given a potential U [56, 57], $\rho \boldsymbol{a} = -\boldsymbol{\nabla} \rho U$, then consider

$$\rho \boldsymbol{u} = \sum_\alpha \boldsymbol{e}_\alpha f_\alpha + \rho \boldsymbol{a} \delta_t = \sum_\alpha \boldsymbol{e}_\alpha f_\alpha + \rho \delta \boldsymbol{u} \tag{2.42}$$

In the Navier-Stokes equation, rewrite [56, 57]

$$-\boldsymbol{\nabla} P + \rho \boldsymbol{a} = -\boldsymbol{\nabla}(\rho\theta + \rho U)\,, \qquad\qquad \delta_t = 1\,. \tag{2.43}$$

Therefore, effectively:

$$P = \rho\theta[1 + U/\theta] \tag{2.44}$$

Equivalent to [up to $O(\delta_t)$]:

$$f_\alpha^{(0)} = f_\alpha^{(0)}(\boldsymbol{u} + \delta \boldsymbol{u}) \tag{2.45}$$

Defects of this model are:

- Lack of equilibrium thermodynamics;
- Incorrect heat transfer ($\rho \boldsymbol{a} \cdot \boldsymbol{u}$ does not affect heat flux $\boldsymbol{q}$).

2.6.3 Modified Model with Interaction Potential

With *a few crude approximations*, such as $f = f^{(0)}$ [28], make

$$\boldsymbol{a} \cdot \boldsymbol{\nabla}_\xi f \approx -\frac{1}{\theta} f^{(0)} (\boldsymbol{\xi} - \boldsymbol{u}) \cdot \boldsymbol{a} \tag{2.46}$$

and assume the forcing:

$$\boldsymbol{a} = -\boldsymbol{\nabla} V - b\rho\theta g \boldsymbol{\nabla} \ln(\rho^2 g) \tag{2.47}$$

where potential V accounts for the attractive component of the intermolecular pairwise potential. The "equation of state" for this model is:

$$P = \rho\theta\,(1 + b\rho g) + V \tag{2.48}$$

This model shares the same defects of the previous one conceptually. In addition, V is redundant — its effect can be included in g.

2.6.4 Model with Free Energy

Use the free energy inspired by Cahn-Hilliard's model

$$\Psi = \int d\boldsymbol{x} \left[\frac{\kappa}{2} \|\boldsymbol{\nabla}\rho\|^2 + \psi(\rho) \right] , \tag{2.49}$$

the the pressure tensor is given by [59, 58]:

$$P = \rho \frac{\delta \Psi}{\delta \rho} - \Psi = p - \kappa \rho \boldsymbol{\nabla}^2 \rho - \frac{\kappa}{2} \|\boldsymbol{\nabla}\rho\|^2 , \tag{2.50a}$$

$$\mathsf{P}_{ij} = P\, \delta_{ij} + \kappa\, \partial_i \rho\, \partial_j \rho . \tag{2.50b}$$

The equation of state is

$$p = \rho \psi' - \psi . \tag{2.51}$$

The equilibrium distribution function is obtained by imposing the following constraint:

$$\sum_\alpha \boldsymbol{e}_{\alpha,i} \boldsymbol{e}_{\alpha,j} f_\alpha^{(\mathrm{eq})} = \mathsf{P}_{ij} \tag{2.52}$$

The equilibrium distribution function satisfied the above constraint is

$$\begin{aligned} f_\alpha^{(\mathrm{eq})} \;=\; & \frac{1}{3}\,\rho \left[1 + (\boldsymbol{e}_\alpha \cdot \boldsymbol{u}) + 2(\boldsymbol{e}_\alpha \cdot \boldsymbol{u})^2 - \frac{1}{2}\boldsymbol{u}^2 \right] \\ & + \frac{\kappa}{3} \left\{ (\boldsymbol{e}_{\alpha,x}^2 - \boldsymbol{e}_{\alpha,y}^2) \left[(\partial_x \rho)^2 - (\partial_y \rho)^2 \right] + 2 \boldsymbol{e}_{\alpha,x} \boldsymbol{e}_{\alpha,y} \partial_x \rho\, \partial_y \rho \right\} \\ & - \frac{\kappa}{3}\, \rho\, \boldsymbol{\nabla}^2 \rho + \frac{1}{3} [\rho \psi'(\rho) - \psi(\rho) - \rho] . \end{aligned} \tag{2.53}$$

There are three parts in the above equilibrium distribution. The first term in brackets [ ] is nothing but the usual equilibrium distribution function of the seven-velocity Frisch-Hasslacher-Pomeau model [15, 25]. The second term in bracket { } is an expression of the tensor $E_{ij} \equiv (\boldsymbol{e}_{\alpha,i} \partial_i \rho)(\boldsymbol{e}_{\alpha,j} \partial_j \rho)$ written in terms of a traceless and an off-diagonal part with correct symmetry such that all the terms proportional to κ reduce to the term $\kappa[\rho \boldsymbol{\nabla}^2 \rho + \|\boldsymbol{\nabla}\rho\|^2/2]$ in the diagonal part of the pressure tensor, given by Eq. (2.50a). This term is directly taken from Cahn-Hilliard's model and it induces surface tension due to density gradient in addition to the part due to the (nonideal gas) equation of state, but it does not contribute to the hydrodynamic pressure (or the equation of state). The nonideal gas part in the equation of state is contained in the last part of the above equation, $[\rho\psi'(\rho) - \psi(\rho) - \rho]/3$, which can be written in a density expansion in general [41, 43]. This term can be viewed as an equivalent forcing term as the following:

$$F_\alpha = \theta[\rho \psi'(\rho) - \psi(\rho)] = \boldsymbol{e}_\alpha \cdot \boldsymbol{\nabla} U . \tag{2.54}$$

The connection between the free-energy model and the interaction model becomes explicit and obvious now. The difference among the two lies in their numerical implementations.

Defects of the free-energy model are:

- Non-Navier-Stokes: lost of Galilean invariance;
- Inconsistent with the Chapman-Enskog analysis;
- Inconsistent thermodynamics: temperature depends on $\boldsymbol{\nabla}\rho$, *etc.*;
- Incorrect heat transfer.

2.6.5 Equivalence of Hamiltonian and Free Energy Approach

Given a Hamiltonian

$$H = \sum_{i=1}^{N} \left[\frac{1}{2} m \boldsymbol{\xi}_i^2 + U(\boldsymbol{r}_i) \right] + \sum_{i<j} V_{ij}(|\boldsymbol{r}_i - \boldsymbol{r}_j|) \tag{2.55}$$

the partition function can be constructed

$$Z = \int d\boldsymbol{r}^N d\boldsymbol{\xi}^N \exp(-H/k_B T) \tag{2.56}$$

then the free energy can be obtained

$$F = -k_B T \ln Z \,. \tag{2.57}$$

Therefore the formalisms of H and F are equivalent — there is gain or lost of information by using one formalism or the other. The difference is that the Hamiltonian H is local whereas the free energy functional F is global. Furthermore, the free-energy density (*e.g.*, $\psi(\rho)$) is local.

2.7 Summary

The conclusions which we can draw are:

- The lattice Boltzmann equation can be directly derived from partial differential equation without being referenced to its historic predecessor — the lattice gas automata.
- The lattice Boltzmann equation is a special finite difference form of the Boltzmann equation. Phase space and time are discretized in a coherent manner such that physical space becomes a lattice space.

- In the lattice Boltzmann equation, the conservation laws are preserved rigorously with discrete momentum space.
- Many numerical techniques for solving PDEs can be used to improve the lattice Boltzmann method.

For the LBE models for nonideal gases, we have discussed three existing LBE models for nonideal gases. We concluded that:

- Lattice Boltzmann for nonideal gases can be derived from the Enskog equation;
- Most existing LBE models are *ad hoc*, and conceptually incorrect;
- Numerics is very important in the interface dynamics.

Lecture 3

The Generalized Lattice Boltzmann Equation

3.1 Motivation

As it is shown, the lattice Boltzmann equation is a special finite difference form of the Boltzmann equation. The most drastic approximation made in the derivation of the lattice Boltzmann equation is the discretization of momentum space $\boldsymbol{\xi}$ into a very small set of discrete velocities $\{\boldsymbol{\xi}_\alpha | \alpha = 1, \ldots, b\}$. The discretization of phase space and time inevitably introduces truncation error and numerical artifacts. It is highly desirable to reduce the effect of the artifacts. In the lattice Boltzmann method, the artifacts due to the following factors are to be analyzed:

- Dissipation due to hyperviscosity. The higher order truncation error would result to hyperviscosty in the LBE hydrodynamics. The hyperviscosity has the following form in general

$$\nu(\boldsymbol{k}) = \nu_0 - \nu_1 k^2 + \nu_2 k^4 + \cdots + (-1)^n \nu_n k^{2n} + \cdots . \tag{3.1}$$

- Galilean Invariance. For any finite difference scheme, Galilean invariance can only be satisfied up to a certain extend. In a reference frame with velocity $\boldsymbol{V}$, the phase of a plain wave is adjusted accordingly:

$$\exp[i(\boldsymbol{k}\cdot\boldsymbol{x} - \omega t)] \Longrightarrow \exp[i(\boldsymbol{k}\cdot\boldsymbol{x} - \omega t) - ig(\boldsymbol{k})\boldsymbol{k}\cdot\boldsymbol{V}t] \tag{3.2}$$

  where g is the Galilean coefficient, which can be expressed as the following:

$$g(\boldsymbol{k}) = g_0 - g_1 k^2 + g_2 k^4 + \cdots + (-1)^n g_n k^{2n} + \cdots . \tag{3.3}$$

  If the system is Galilean invariant, then we must have $g = 1$.

- Isotropy. Discretization causes anisotropic effect, that is, the transport coefficients, the shear viscosity $\nu(\boldsymbol{k})$, the bulk viscosity $\eta(\boldsymbol{k})$, the sound speed $c_s(\boldsymbol{k})$, and the Galilean coefficient $g(\boldsymbol{k})$, all depend on the direction of wave vector $\boldsymbol{k}$.

We propose to studies the generalized hydrodynamics [39, 21] of the lattice Boltzmann equation by a systematic analysis of the linearized dispersion equation of the lattice Boltzmann equation [37]. The analysis would help us to optimize the lattice Boltzmann method in terms of reducing its affects.

3.2 The Lattice Boltzmann Equation in Moment Space

The lattice Boltzmann equation in particle velocity space is

$$f_\alpha(\boldsymbol{x}_i + \boldsymbol{e}_\alpha,\, t+1) = f_\alpha(\boldsymbol{x}_i,\, t) + \Omega_\alpha(f)\,. \tag{3.4}$$

The hydrodynamic moments are computed from $\{f_\alpha\}$ as follows:

$$\rho(\boldsymbol{x}_i,\, t) \;=\; \sum_\alpha f_\alpha(\boldsymbol{x}_i,\, t)\,, \tag{3.5a}$$

$$\rho\boldsymbol{u}(\boldsymbol{x}_i,\, t) \;=\; \sum_\alpha \boldsymbol{e}_\alpha f_\alpha(\boldsymbol{x}_i,\, t)\,. \tag{3.5b}$$

The lattice Boltzmann equation (3.4) can be rewritten in a concise vector form:

$$|f(\boldsymbol{x}_i + \boldsymbol{e}_\alpha,\, t+1)\rangle = |f(\boldsymbol{x}_i,\, t)\rangle + |\Omega(f)\rangle \tag{3.6}$$

where the Dirac notations of bra $\langle\cdot|$ for row vector and ket $|\cdot\rangle$ for column vector are used,

$$|f(\boldsymbol{x}_j)\rangle \equiv (f_0,\, f_1,\, \ldots, f_8)^{\mathsf{T}}\,, \tag{3.7a}$$

$$|f(\boldsymbol{x}_j + \boldsymbol{e}_\alpha, t+1)\rangle \equiv (f_0(\boldsymbol{x}_j + \boldsymbol{e}_0, t+1),\, \ldots,\, f_8(\boldsymbol{x}_j + \boldsymbol{e}_8, t+1))^{\mathsf{T}}\,, \tag{3.7b}$$

$$|\Omega(f)\rangle \equiv (\Omega_0(f),\, \Omega_1(f),\, \ldots,\, \Omega_8(f))^{\mathsf{T}}\,, \tag{3.7c}$$

and T is the transpose operator.

Given a set of b discrete velocities, $\{\boldsymbol{e}_\alpha | \alpha = 0,\, 1,\, \ldots,\, (b-1)\}$, with corresponding distribution functions, $\{f_\alpha | \alpha = 0,\, 1,\, \ldots,\, (b-1)\}$, one can construct a b-dimensional vector space $\mathbb{V} = \mathbb{R}^b$ based upon the discrete velocity set. One can also construct a space $\mathbb{M} = \mathbb{R}^b$ based upon the (velocity) moments of $\{f_\alpha\}$. Obviously, there are b independent moments for the discrete velocity set. The reason in favor of using the moment representation over the distribution function representation is somewhat obvious. It is well understood in the context of kinetic theory that various physical processes in fluids, such as viscous transport, can be approximately described by coupling or interaction among 'modes' (of the collision operator), and these modes are directly related to the moments (*e.g.*, the hydrodynamic modes are linear combinations of mass, and momenta moments). Thus the moment representation provides a convenient and effective means by which to incorporate the physics into the LBE models. Because the physical significance of the moments is obvious (hydrodynamic quantities and their fluxes, *etc.*), the relaxation parameters of the moments are directly related to the various transport coefficients. This mechanism allows us to control each mode independently. This also overcomes some obvious deficiencies of the usual BGK LBE model, such as a fixed Prandtl number, which is due to a single relaxation parameter of the model.

For the nine-velocity LBE model on a square lattice in two-dimensions, the following mapping

$$\begin{aligned}
\mathsf{M} &\equiv \begin{pmatrix} \langle\rho| \\ \langle e| \\ \langle\varepsilon| \\ \langle j_x| \\ \langle q_x| \\ \langle j_y| \\ \langle q_y| \\ \langle p_{xx}| \\ \langle p_{xy}| \end{pmatrix} \equiv \begin{pmatrix} 1 & 1 & 1 & 1 & 1 & 1 & 1 & 1 & 1 \\ -4 & -1 & -1 & -1 & -1 & 2 & 2 & 2 & 2 \\ 4 & -2 & -2 & -2 & -2 & 1 & 1 & 1 & 1 \\ 0 & 1 & 0 & -1 & 0 & 1 & -1 & -1 & 1 \\ 0 & -2 & 0 & 2 & 0 & 1 & -1 & -1 & 1 \\ 0 & 0 & 1 & 0 & -1 & 1 & 1 & -1 & -1 \\ 0 & 0 & -2 & 0 & 2 & 1 & 1 & -1 & -1 \\ 0 & 1 & -1 & 1 & -1 & 0 & 0 & 0 & 0 \\ 0 & 0 & 0 & 0 & 0 & 1 & -1 & 1 & -1 \end{pmatrix} \\
&\equiv (|\rho\rangle, |e\rangle, |\varepsilon\rangle, |j_x\rangle, |q_x\rangle, |j_y\rangle, |q_y\rangle, |p_{xx}\rangle, |p_{xy}\rangle)^{\mathsf{T}}
\end{aligned} \tag{3.8}$$

uniquely maps a vector $|f\rangle$ in discrete velocity space $\mathbb{V} = \mathbb{R}^b$ to a vector $|\varrho\rangle$ in moment space $\mathbb{M} = \mathbb{R}^b$, and *vice versa*, that is

$$|\varrho\rangle = \mathsf{M}|f\rangle\,, \qquad |f\rangle = \mathsf{M}^{-1}|\varrho\rangle\,. \tag{3.9}$$

Note that the row vectors in M have explicit physical significances related to the moments of $\{f_\alpha\}$ in discrete velocity space: $|\rho\rangle$ is the density mode; $|e\rangle$ is the energy mode; $|\varepsilon\rangle$ is related to energy square; $|j_x\rangle$ and $|j_y\rangle$ correspond to the x and y components of momentum (mass flux); $|q_x\rangle$ and $|q_y\rangle$ correspond to the x and y components of energy flux; and $|p_{xx}\rangle$ and $|p_{xy}\rangle$ correspond to the diagonal and off-diagonal components of the stress tensor.

The moments for the nine-velocity model are:

Order	Quantity	Moment
0	Density:	$\rho = \langle\rho\|f\rangle = \langle f\|\rho\rangle\,,$
2	Energy:	$e = \langle e\|f\rangle = \langle f\|e\rangle$
4	Energy Square:	$\varepsilon = \langle\varepsilon\|f\rangle = \langle f\|\varepsilon\rangle\,,$
1	x-Momentum:	$j_x = \langle j_x\|f\rangle = \langle f\|j_x\rangle\,,$
3	x-Heat Flux:	$q_x = \langle q_x\|f\rangle = \langle f\|q_x\rangle\,,$
1	y-Momentum:	$j_y = \langle j_y\|f\rangle = \langle f\|j_y\rangle\,,$
3	y-Heat Flux:	$q_y = \langle q_y\|f\rangle = \langle f\|q_y\rangle\,,$
2	Diagonal stress:	$p_{xx} = \langle p_{xx}\|f\rangle = \langle f\|p_{xx}\rangle\,,$
2	Off-diagonal stress:	$p_{xy} = \langle p_{xy}\|f\rangle = \langle f\|p_{xy}\rangle\,.$

3.3 The Generalized BGK Approximation in Moment Space

Instead of the single relaxation time approximation, one can use multiple relaxation times approximation. This is a generalization of the BGK approximation [31, 8].

For the nine-velocity LBE model, at most there can be six independent relaxation parameters because there are only six kinetic (non-conservative) modes in the model. Therefore, the relaxation process can be cast as the following

$$\begin{pmatrix} \Delta\rho \\ \Delta e \\ \Delta\varepsilon \\ \Delta j_x \\ \Delta q_x \\ \Delta j_y \\ \Delta q_y \\ \Delta p_{xx} \\ \Delta p_{xy} \end{pmatrix} = \begin{pmatrix} 0 & 0 & 0 & 0 & 0 & 0 & 0 & 0 & 0 \\ 0 & -s_2 & 0 & 0 & 0 & 0 & 0 & 0 & 0 \\ 0 & 0 & -s_3 & 0 & 0 & 0 & 0 & 0 & 0 \\ 0 & 0 & 0 & 0 & 0 & 0 & 0 & 0 & 0 \\ 0 & 0 & 0 & 0 & -s_5 & 0 & 0 & 0 & 0 \\ 0 & 0 & 0 & 0 & 0 & 0 & 0 & 0 & 0 \\ 0 & 0 & 0 & 0 & 0 & 0 & -s_7 & 0 & 0 \\ 0 & 0 & 0 & 0 & 0 & 0 & 0 & -s_8 & 0 \\ 0 & 0 & 0 & 0 & 0 & 0 & 0 & 0 & -s_9 \end{pmatrix} \begin{pmatrix} \delta\rho \\ \delta e \\ \delta\varepsilon \\ \delta j_x \\ \delta q_x \\ \delta j_y \\ \delta q_y \\ \delta p_{xx} \\ \delta p_{xy} \end{pmatrix} \tag{3.10}$$

where $\Delta\varrho_\alpha$ denotes the change of the moment ϱ_α due to collision (or relaxation), while $\delta\varrho_\alpha$ denotes the deviation from the equilibrium. In vector notation, we have

$$|\delta\varrho\rangle \equiv |\varrho\rangle - |\varrho^{(\mathrm{eq})}\rangle\,, \tag{3.11a}$$

$$|\Delta\varrho\rangle = \mathsf{S}\,|\delta\varrho\rangle\,. \tag{3.11b}$$

3.4 The Equilibria in Moment Space

The equilibrium distribution functions depend only upon conserved moments:

$$e^{(\mathrm{eq})} = \frac{1}{\langle e|e\rangle}\left[\alpha_2\,\langle\rho|\rho\rangle\,\rho + \gamma_2\,(\langle j_x|j_x\rangle j_x^2 + \langle j_y|j_y\rangle j_y^2)\right] \tag{3.12a}$$

$$= \frac{1}{4}\alpha_2\,\rho + \frac{1}{6}\gamma_2\,(j_x^2 + j_y^2)\,,$$

$$\varepsilon^{(\mathrm{eq})} = \frac{1}{\langle\varepsilon|\varepsilon\rangle}\left[\alpha_3\,\langle\rho|\rho\rangle\,\rho + \gamma_4\,(\langle j_x|j_x\rangle j_x^2 + \langle j_y|j_y\rangle j_y^2)\right] \tag{3.12b}$$

$$= \frac{1}{4}\alpha_3\,\rho + \frac{1}{6}\gamma_4\,(j_x^2 + j_y^2)\,,$$

$$q_x^{(\mathrm{eq})} = \frac{\langle j_x|j_x\rangle}{\langle q_x|q_x\rangle}c_1 j_x = \frac{1}{2}c_1 j_x\,, \tag{3.12c}$$

$$q_y^{(\mathrm{eq})} = \frac{\langle j_y|j_y\rangle}{\langle q_y|q_y\rangle}c_1 j_y = \frac{1}{2}c_1 j_y\,, \tag{3.12d}$$

$$p_{xx}^{(\mathrm{eq})} = \gamma_1\,\frac{1}{\langle p_{xx}|p_{xx}\rangle}(\langle j_x|j_x\rangle j_x^2 - \langle j_y|j_y\rangle j_y^2) = \frac{3}{2}\gamma_1(j_x^2 - j_y^2)\,, \tag{3.12e}$$

$$p_{xy}^{(\mathrm{eq})} = \gamma_3\,\frac{\sqrt{\langle j_x|j_x\rangle\langle j_y|j_y\rangle}}{\langle p_{xx}|p_{xx}\rangle}(j_x j_y) = \frac{3}{2}\gamma_3(j_x j_y)\,. \tag{3.12f}$$

There are seven adjustable parameters in the model: α_2, α_3, c_1, γ_1, γ_2, γ_3, γ_4. These parameters will be determined by the analysis of the linearized dispersion equation [37].

3.5 The Generalized Lattice Boltzmann Equation

The generalized lattice Boltzmann equation with multiple relaxation parameters is written as [8, 37]

$$|f(\boldsymbol{x}_i + \boldsymbol{e}_\alpha,\, t+1)\rangle = |f(\boldsymbol{x}_i,\, t)\rangle + \mathsf{M}^{-1}\mathsf{S}\left[|\varrho(\boldsymbol{x}_i,\, t)\rangle - |\varrho^{(\mathrm{eq})}(\boldsymbol{x}_i,\, t)\rangle\right]. \tag{3.13}$$

The computation of the generalized lattice Boltzmann equation involves the following steps (after the initialization of $|f\rangle$):

- Project $|f\rangle$ to moments by $|\varrho\rangle = \mathsf{M}|f\rangle$, and compute the equilibrium $|\varrho^{(\mathrm{eq})}\rangle$;
- Collision in moment space (multiple-parameter relaxation)

$$|\Delta\varrho\rangle \equiv \mathsf{S}\left[|\varrho\rangle - |\varrho^{(\mathrm{eq})}\rangle\right];$$

- Project $|\varrho\rangle$ back to $|f\rangle = \mathsf{M}^{-1}|\varrho\rangle$ to perform advection step in velocity space:

$$|f(\boldsymbol{x}_i + \boldsymbol{e}_\alpha,\, t+1)\rangle = |f(\boldsymbol{x}_i,\, t)\rangle + \mathsf{M}^{-1}|\Delta\varrho\rangle.$$

The computational overhead due to the projections between $\mathbb{V}$ and $\mathbb{M}$ is not heavy. It is generally about 10 – 20% of the of the LBGK algorithm.

3.6 The Linearized Lattice Boltzmann Equation

Suppose the system in uniform state of ρ and $\boldsymbol{V} = (V_x,\, V_y)$, and

$$|f\rangle = |f^{(0)}\rangle + |\delta f\rangle. \tag{3.14}$$

The lattice Boltzmann equation can be linearized:

$$|\delta f(\boldsymbol{x}_j + \boldsymbol{e}_\alpha,\, t+1)\rangle = |\delta f(\boldsymbol{x}_j,\, t)\rangle + \mathsf{M}^{-1}\mathsf{C}\mathsf{M}|\delta f(\boldsymbol{x}_j,\, t)\rangle. \tag{3.15}$$

In Fourier space, the above linearized LBE becomes

$$\mathsf{A}|\delta f(\boldsymbol{k},\, t+1)\rangle = |\delta f(\boldsymbol{k},\, t)\rangle + \mathsf{M}^{-1}\mathsf{C}\mathsf{M}|\delta f(\boldsymbol{k},\, t)\rangle, \tag{3.16}$$

where the linearized collision operator C and the advection operator A are given by:

$$\mathsf{C}_{\alpha\beta} = \frac{\langle\varrho_\alpha|\varrho_\alpha\rangle}{\langle\varrho_\beta|\varrho_\beta\rangle}\frac{\partial}{\partial\varrho_\alpha}\left[\varrho_\beta - \varrho_\beta^{(\mathrm{eq})}\right], \tag{3.17a}$$

$$\mathsf{A}_{\alpha\beta} = \exp(i\boldsymbol{e}_\alpha\cdot\boldsymbol{k})\,\delta_{\alpha\beta}. \tag{3.17b}$$

The linearized lattice Boltzmann equation can be written as the following:

$$|\delta f(\boldsymbol{k},\, t+1)\rangle = \mathsf{L}|\delta f(\boldsymbol{k},\, t)\rangle, \tag{3.18}$$

where L is the linearized evolution operator:

$$\mathsf{L} = \mathsf{A}^{-1}[\mathsf{I} + \mathsf{M}^{-1}\mathsf{C}\mathsf{M}]. \tag{3.19}$$

3.7 Eigenvalue Problem of the Linearized Lattice Boltzmann Equation

The solution of the linearized lattice Boltzmann equation is equivalent to an eigenvalue problem of the linearized evolution operator:

$$\det[\mathsf{L} - z\mathsf{I}] = 0\,. \tag{3.20}$$

Hydrodynamic modes (corresponding to $z_\alpha = 1$) of L at $\boldsymbol{k} = (k\cos\theta,\, k\sin\theta) \to \boldsymbol{0}$ are one transverse (shear) mode and two longitudinal (sound) modes:

$$|\varrho_T\rangle = \cos\theta|j_x\rangle - \sin\theta|j_y\rangle \equiv |j_T\rangle\,, \tag{3.21a}$$

$$|\varrho_\pm\rangle = |\rho\rangle \pm (\cos\theta|j_x\rangle + \sin\theta|j_y\rangle) \equiv |\rho\rangle \pm |j_L\rangle\,. \tag{3.21b}$$

When $\boldsymbol{k} \neq \boldsymbol{0}$, we have

$$|\varrho_T(t)\rangle = {z_T}^t\,|\varrho_T(0)\rangle = \exp[-ik(gV\cos\phi)t]\exp(-\nu k^2 t)|\varrho_T(0)\rangle\,, \tag{3.22a}$$

$$\begin{aligned}|\varrho_\pm(t)\rangle &= {z_\pm}^t\,|\varrho_\pm(0)\rangle \\ &= \exp[\pm ik(c_s \pm gV\cos\phi)t]\exp[-(\nu/2+\zeta)k^2 t]|\varrho_\pm(0)\rangle\,.\end{aligned} \tag{3.22b}$$

Transport coefficients ν, ζ, c_s, and g are functions of wavevector $\boldsymbol{k}$, and the adjustable parameters in the model [see Eqs. (3.12)]. By optimizing the isotropy of the transport coefficients and minimizing the non-Galilean effect of the model, the values of the adjustable parameters can be determined.

3.8 Determination of the Adjustable Parameters

The Galilean invariance of the phases in the transverse mode (z_T) and the sound modes ($z_\pm$) up to $\boldsymbol{k}$ leads to:

$$\gamma_1 = \gamma_3 = \frac{2}{3}\,, \tag{3.23a}$$

$$\gamma_2 = 18\,. \tag{3.23b}$$

Isotropy of the attenuation of the transverse mode (z_T) and the Galilean invariance of the attenuation of the sound modes ($z_\pm$) lead to

$$c_1 = -2\,, \qquad (\text{equivalent to } c_s = 1/\sqrt{3})\,, \tag{3.24a}$$

$$\alpha_2 = -8\,. \tag{3.24b}$$

The remaining adjustable parameters are: α_3 and γ_4 (in $\epsilon^{(\mathrm{eq})}$). If we chose

$$\alpha_3 = 4\,, \tag{3.25a}$$

$$\gamma_4 = -18\,, \tag{3.25b}$$

and $s_\alpha = 1/\tau$, the generalized lattice Boltzmann equation reduces to a lattice BGK model.

3.9 Behaviors of Eigenvalues of the Linearized Collision Operator L

The behaviors of eigenvalues of the linearized collision operator L determine the local stability of the LBE model: If $\mathrm{Re}(\ln z_\alpha) > 0$, then the corresponding mode $|\varrho_\alpha\rangle$ is unstable. Figure 3.1 shows the real and imaginary parts of the nine roots of L with a given set of parameters. It shows that when $k = \pi$, one kinetic mode becomes "quasi-conservative," because the corresponding eigenvalue is equal to 1 when $k = \pi$. This is the mode which generates the checker-board pattern and instigates instability at short wave length.

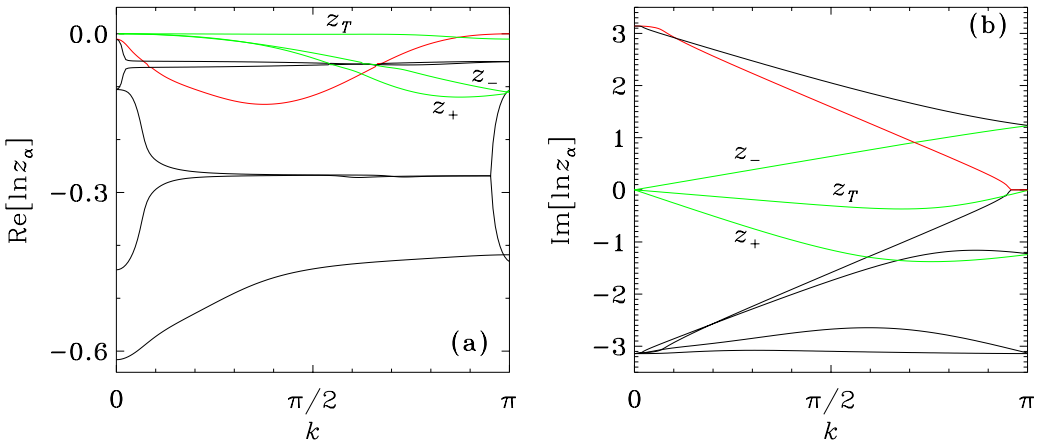

Figure 3.1: Logarithmic eigenvalues of the nine-velocity model. The values of the parameters are $\alpha_2 = -8$, $\alpha_3 = 4$, $c_1 = -2$, $\gamma_1 = \gamma_3 = 2/3$, $\gamma_2 = 18$, and $\gamma_4 = -18$. The relaxation parameters are: $s_2 = 1.64$, $s_3 = 1.54$, $s_5 = s_7 = 1.9$, and $s_8 = s_9 = 1.99$. The streaming velocity $\boldsymbol{V}$ is parallel to $\boldsymbol{k}$ with $V = 0.2$, and $\boldsymbol{k}$ is along the x axis. (a) $\mathrm{Re}(\ln z_\alpha)$ and (b) $\mathrm{Im}(\ln z_\alpha)$.

The adjustable parameters in our model can be used to alter the properties of the model. The stability of the BGK LBE model and our model is compared in Fig. 3.2. In this case we choose the adjustable parameters in our model to be the same as the BGK LBE model, but maintain the freedom of different modes to relax with different relaxation parameters s_α. Figure 3.2 shows that for each given value of $\boldsymbol{V}$, there exists a maximum value of $s_8 = 1/\tau$ (which determines the shear viscosity) below which there is no unstable mode. The values of other relaxation parameters used in our model are $s_2 = 1.63$, $s_3 = 1.14$, $s_5 = s_7 = 1.92$, and $s_9 = s_8 = 1/\tau$. Figure 3.2 clearly shows that our model is more stable than the BGK LBE model in the interval $1.9 \leq s_8 = 1/\tau \leq 1.99$. Therefore, we can conclude that by carefully separating the kinetic modes with different relaxation rates, we can indeed improve the stability of the LBE model significantly.

The behaviors of transport coefficients are also determined by the eigenvalues of

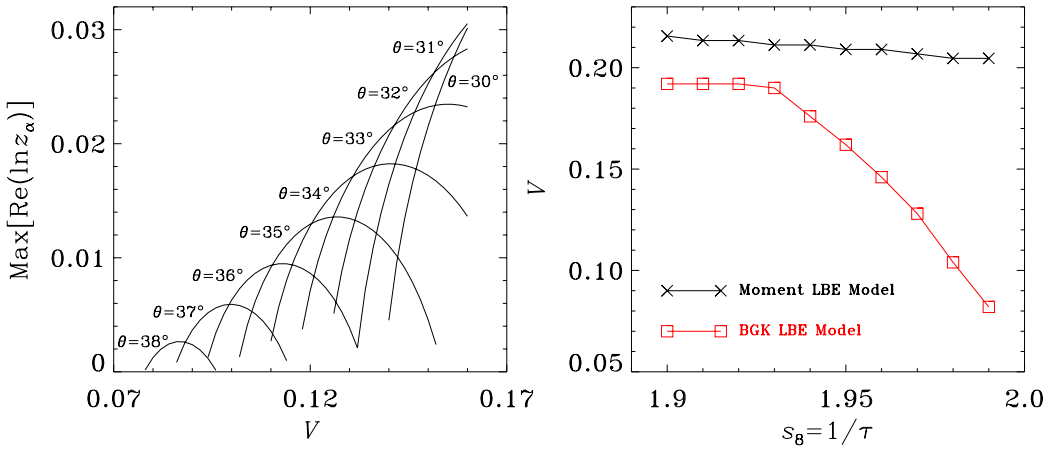

Figure 3.2: Stability of the generalized LBE model *vs.* the BGK LBE model in the parameter space of V and $s_8 = 1/\tau$. (left) $\max[\mathrm{Re}(\ln z_\alpha)]$ for given $\boldsymbol{V}$. (right) Stability region of GLBE *vs.* LBGK model.

L. Figure 3.3 shows the $\boldsymbol{k}$-dependence of the viscosity and the Galilean coefficient g. It shows that in small scales (large k), the LBE model becomes more anisotropic and non-Galilean invariant. In addition, the use of interpolation significantly increases the hyperviscosity and the effect of non-Galilean invariance.

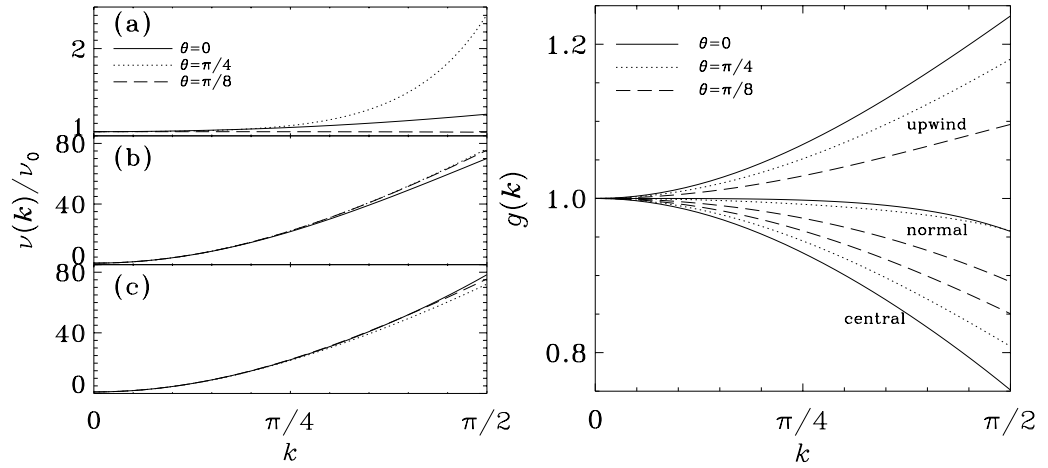

Figure 3.3: $\boldsymbol{k}$-dependence of viscosities and g-factor. The solid lines, dotted lines, and dashed lines correspond to $\theta = 0$, $\pi/8$, and $\pi/4$, respectively. Three LBE model tested: (a) with no interpolation, (a) with central interpolation, and (c) with upwind interpolation.

The artifacts of the LBE method can also be analyzed. We study an interesting and revealing case in which the initial velocity field contains shocks. Consider a periodic domain of size $N_x \times N_y = 84 \times 4$. At time $t = 0$, we take a shear wave

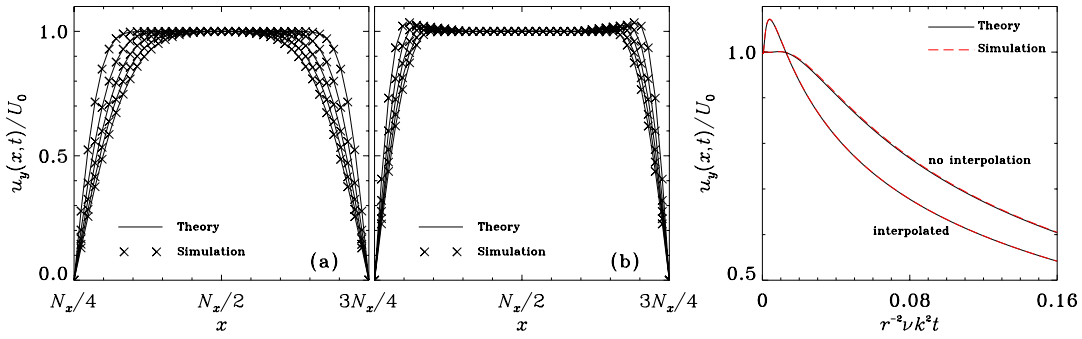

Figure 3.4: Decay of discontinuous shear wave velocity profile $u_y(x,\, t)$. (left) The lines and symbols ($\times$) are theoretical and numerical results, respectively. Only the positive half of each velocity profile is shown. LBE model (a) with no interpolation, (b) with the central interpolation and $r = 0.5$. (right) Decay of $u_y(x,\, t)$ at a location close to the discontinuity $x = 3N_x/4$. The solid lines and dashed lines are analytic and numerical results, respectively. The time is rescaled as $r^{-2}\nu k^2 t$.

$u_y(x,\, 0)$ of rectangular shape (discontinuities in u_y at $x = N_x/4$ and $x = 3N_x/4$):

$$\begin{aligned} u_y(x,\, 0) &= U_0, \qquad 1 < x \le N_x/4, \quad 3N_x/4 < x \le N_x, \\ u_y(x,\, 0) &= -U_0, \qquad N_x/4 < x \le 3N_x/4. \end{aligned}$$

The initial condition $u_x(x,\, 0)$ is set to zero everywhere. We consider two separate cases with and without a constant streaming velocity $\boldsymbol{V}$.

Figures 3.4(a) and 3.4(b) show the decay of the rectangular shear wave simulated by the normal LBE scheme and the LBE scheme with second-order central interpolation (with $r = 0.5$, where r is the ratio between advection length δ_x and grid size Δ_x), respectively. The lines are theoretical results with $\nu(k_n)$ obtained numerically. The times at which the profile of $u_y(x,\, t)$ (normalized by U_0) shown in Fig. 3.4 are $t = 100,\, 200,\, \ldots,\, 500$. The numerical and theoretical results agree closely with each other. The close agreement shows the accuracy of the theory. In Fig. 3.4(b), the overshoots at early times due to the discontinuous initial condition are well captured by the analysis. This overshoot is entirely due to the strong $\boldsymbol{k}$-dependence of $\nu(\boldsymbol{k})$ caused by the interpolation. This phenomena is an artifact due to discretization, and is not connected to any physical effect. This artifact is also commonly observed in other CFD methods involving interpolations.

Similarly to Fig. 3.4, Fig. 3.5 shows the evolution of $u_y(x,\, t)$ for the same times as in Fig. 3.4. The solid lines and the symbols ($\times$) represent theoretical and numerical results, respectively. Shocks move from left to right with a constant velocity $V_x = 0.08$. Figures 3.5(a), 3.5(b), and 3.5(c) show the results for the normal LBE scheme without interpolation, the scheme with second-order central interpolation, and the scheme with second-order upwind interpolation, respectively. In Figs. 3.5(b) and

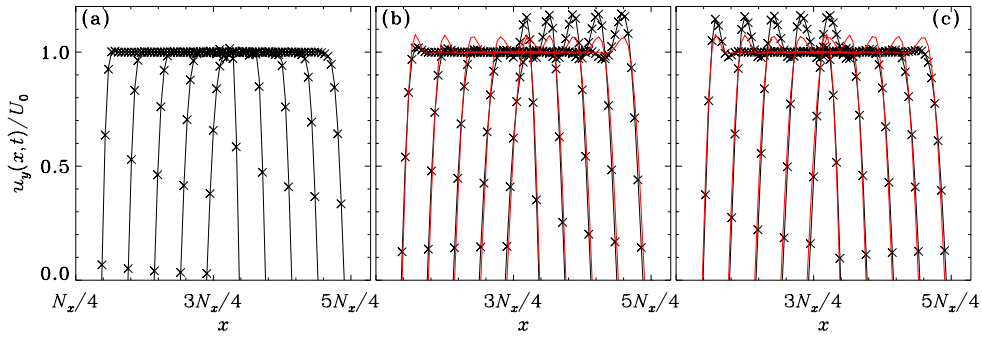

Figure 3.5: Decay of discontinuous shear wave velocity profile $u_y(x,\, t)$ with a constant streaming velocity $V_x = 0.08 = U_0$. The solid lines and symbols ($\times$) are theoretical and numerical results, respectively. The dashed lines in (b) and (c) are obtained by setting $g_n = 1$. (a) no interpolation, (b) central interpolation and $r = 0.5$, (c) upwind interpolation and $r = 0.5$.

3.5(c), the dotted lines are the results obtained by setting $g_n = 1$. Clearly, the effect of $g(\boldsymbol{k})$ is significant. For the LBE scheme with central interpolation, the results in Fig. 3.5(b) with $g(\boldsymbol{k}) = 1$ underpredict the overshooting at the leading edge of the shock and overpredict the overshooting at the trailing edge, whereas the results in Fig. 3.5(c) for the LBE scheme with upwind interpolation overpredict the overshooting at the leading edge of the shock and underpredict the overshooting at the trailing edge.

3.10 Summary

We have constructed a generalized LBE model with multiple relaxation times. The hydrodynamic behavior of the model is obtained by analyzing the linearized dispersion equation. Based on our analysis, we can draw the following conclusions:

- The generalized LBE is superior than the Lattice BGK model in terms of stability, isotropy, and Galilean invariance. The Prandtl number of the generalized LBE can be arbitrary;
- Analysis of the linearized dispersion equation is equivalent to the Chapman-Enskog analysis, while Chapman-Enskog analysis is not valid for situation of finite wavevector $\boldsymbol{k}$;
- Analysis of the linearized dispersion equation is also applicable to complex fluids (*e.g.*, viscoelastic fluids).

We also realize the limitations of the dispersion equation analysis. It cannot deal with nonlocal effects (gradients) and the boundary conditions. A detailed treatment of the generalized lattice Boltzmann equation is provided in Ref. [37].

Lecture 4

Boundary Conditions in LBE Method and Applications

Fluid-solid boundary condition, and other types of boundary conditions are important in CFD simulations. In the LBE method, the primitive variables are the distribution functions $\{f_\alpha\}$, but not the hydrodynamic variables ρ, $\boldsymbol{u}$, and T. Accordingly, the boundary conditions in the LBE simulations are imposed on the distribution functions $\{f_\alpha\}$, and only on the hydrodynamic variables *indirectly*. This is one of the most distinctive features of the LBE methods, as compared to the conventional CFD methods which are based on the discretizations of the Navier-Stokes equations. We shall discuss one of most popular fluid-solid boundary conditions in the LBE method: bounce-back boundary conditions.

4.1 Bounce-Back Boundary Conditions

The bounce-back boundary conditions were first used in the lattice-gas to mimic the no-slip boundary conditions on a fluid-solid surface. The idea is very simple and intuitive as the name suggests: when a particle hits on a solid surface, it simply reverses its momentum.

The bounce-back boundary conditions can be easily adopted in the LBE method. Suppose a lattice site $\boldsymbol{x}_b$ is designated as a solid site on a boundary, the bounce-back boundary conditions can be simply expressed as

$$f_\alpha(\boldsymbol{x}_j, *) = f_{\bar{\alpha}}(\boldsymbol{x}_b, *), \qquad \forall\ \boldsymbol{x}_j,\ \{\boldsymbol{x}_j | \boldsymbol{x}_j + \boldsymbol{e}_\alpha \delta_t = \boldsymbol{x}_b\}. \tag{4.1}$$

The time argument in the above formula is deliberately omitted because the bounce-back collision process can be thought to take place either simultaneously or in one time step. This leads two implementations of the bounce-back boundary conditions, with the difference of one time step between the outgoing (from fluid to solid) and incoming (from solid to fluid) states. This makes no difference for steady-state situations. However, the spatial-temporal symmetry of these two implementations are different: one (no time lag) destroys and the other (with one time step lag) preserves the checker-board spatial symmetry, and this may affect the numerical stability of the LBE methods near the boundary [37].

The implementations of the bounce-back boundary conditions in the LBE methods can have some variations. For instance, one can relax the distribution functions

at the boundary nodes to the equilibria with the velocity imposed by the flow boundary conditions [29].

One most important feature of the bounce-back boundary conditions is that the flow boundary conditions cannot be satisfied on the last fluid nodes next to the solid boundaries (nodes). The flow boundary conditions are satisfied some where between a fluid node and a solid node. For simple flows, such as the Couette flow or Poiseuille flow, the exact location where the flow boundary conditions are satisfied are known analytically [39, 16, 17, 40, 29], if the boundaries are aligned with the lattice.

Despite of its simplicity, the bounce-back boundary conditions are sufficiently accurate, *i.e.*, it is second-order accurate. However, the bounce-back scheme approximates any continuous curve/surface with a zig-zag staircase. This practice degrades the geometric integrity of a continuous boundary. We shall discuss how to improve the preservation of the geometric integrity of a continuous boundary next.

4.2 Bounce-Back Boundary Conditions with Interpolations

In the LBE method, the fluid simulation is conducted on a Eulerian Cartesian mesh, which is fixed in space and time. If a body moving in fluid has to be considered, then the Lagrangian dynamics has to be used to describe the motion of the moving body, *i.e.*, the coordinate system associated with the body is moving with respect to the Eulerian coordinate system for the fluids. Thus, there are two different methodologies in general: (1) body-fitted meshes and (2) Cartesian meshes with immersed body method (IBM); and the LBE treatment of solid-boundaries belongs to the latter methodology. Figure 4.1 depicts the basic ideas in the LBE-IBM treatment of a curved boundary.

In order to improve the quality of the bounce-back boundary treatment, the precise boundary location must be resolved within one grid spacing. The simplest way to accomplish this is to introduce interpolations at the boundary.

With the picture for the simple bounce-back scheme in mind, let's first consider the situation depicted in Fig. 4.2b in detail for the case of $\Delta < 1/2$. At time t the distribution function of the particle with velocity pointing to the wall ($\boldsymbol{e}_1$ in Fig. 4.2) at the grid point $\boldsymbol{x}_j$ (a fluid node) would end up at the point $\boldsymbol{x}_i$ located at a distance $(1-2\Delta)\delta_x$ away from the grid point $\boldsymbol{x}_j$, after the bounce-back collision, as indicated by the thin bent arrow in Fig. 4.2b. Because $\boldsymbol{x}_i$ is not a grid point, the value of f_3 at the grid point $\boldsymbol{x}_j$ needs to be reconstructed. Noticing that f_1 starting from point $\boldsymbol{x}_i$ would become f_3 at the grid point $\boldsymbol{x}_j$ after the bounce-back collision with the wall, we construct the values of f_1 at the point $\boldsymbol{x}_i$ by a quadratic interpolation involving values of f_1 at the three locations: $f_1(\boldsymbol{x}_j), f_1(\boldsymbol{x}_{j'}) = f_1(\boldsymbol{x}_j - \boldsymbol{e}_1\delta_t)$, and $f_1(\boldsymbol{x}_{j''}) = f_1(\boldsymbol{x}_j - 2\boldsymbol{e}_1\delta_t)$. In a similar manner, for the case of $\Delta \geq 1/2$ depicted in Fig. 4.2c, we can construct $f_3(\boldsymbol{x}_j)$ by a quadratic interpolation involving $f_3(\boldsymbol{x}_i)$ that is equal to $f_1(\boldsymbol{x}_j)$ before the bounce-back collision, and the values of f_3 at the nodes after collision and advection, i.e., $f_3(\boldsymbol{x}_{j'})$, and $f_3(\boldsymbol{x}_{j''})$. Therefore the interpolations

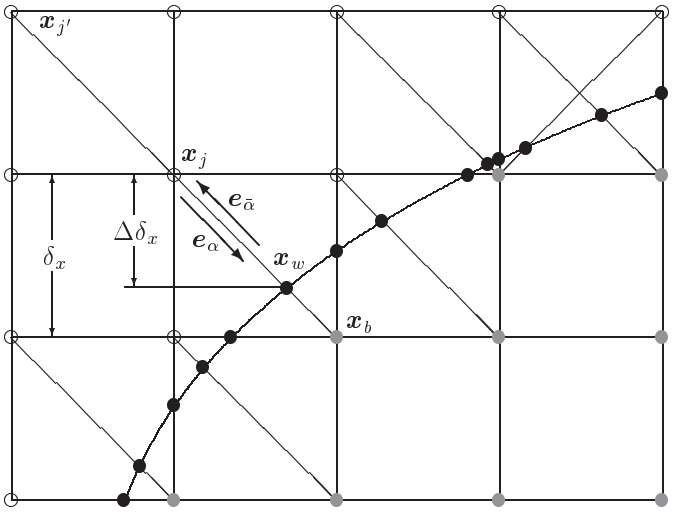

Figure 4.1: Layout of the regularly spaced lattices and curved wall boundary. The circles ($\circ$), discs ($\bullet$), shaded discs ($\bullet$), and diamonds ($\diamond$) denote fluid nodes, boundary locations ($\boldsymbol{x}_w$), solid nodes which are also boundary nodes ($\boldsymbol{x}_b$) inside solid, and solid nodes, respectively.

are applied differently for the two cases:

- For $\Delta < 1/2$, interpolate before propagation and bounce-back collision;
- For $\Delta \geq 1/2$, interpolate after propagation and bounce-back collision.

We do so to avoid the use of extrapolations in the boundary conditions for the sake of numerical stability. This leads to the following interpolation formulas (where the notations $\hat{f}_\alpha$ and f_α denote the post-collision distribution functions before and after advection):

$$f_{\bar{\alpha}}(\boldsymbol{x}_j, t) = \Delta\,(1+2\,\Delta)\hat{f}_\alpha(\boldsymbol{x}_j, t) + (1-4\,\Delta^2)\hat{f}_\alpha(\boldsymbol{x}_{j'}, t) \\ -\Delta\,(1-2\,\Delta)\hat{f}_\alpha(\boldsymbol{x}_{j''}, t) + 3w_\alpha(\boldsymbol{e}_\alpha \cdot \boldsymbol{u}_w)\,, \qquad \Delta < \frac{1}{2}, \tag{4.2a}$$

$$f_{\bar{\alpha}}(\boldsymbol{x}_j, t) = \frac{1}{\Delta\,(2\,\Delta+1)}\hat{f}_\alpha(\boldsymbol{x}_j, t) + \frac{(2\,\Delta-1)}{\Delta}f_{\bar{\alpha}}(\boldsymbol{x}_{j'}, t) \\ -\frac{(2\,\Delta-1)}{(2\,\Delta+1)}f_{\bar{\alpha}}(\boldsymbol{x}_{j''}, t) + \frac{3w_\alpha}{\Delta\,(2\,\Delta+1)}(\boldsymbol{e}_\alpha \cdot \boldsymbol{u}_w)\,, \quad \Delta \geq \frac{1}{2}\,, \tag{4.2b}$$

$$w_\alpha = \begin{cases} 2/9, & \alpha = 1-4, \\ 2/36, & \alpha = 5-8, \end{cases} \tag{4.2c}$$

In practice, it is more efficient to combine collision and advection into one step. Because advection simply corresponds to shifts of indices labeling spatial nodes of

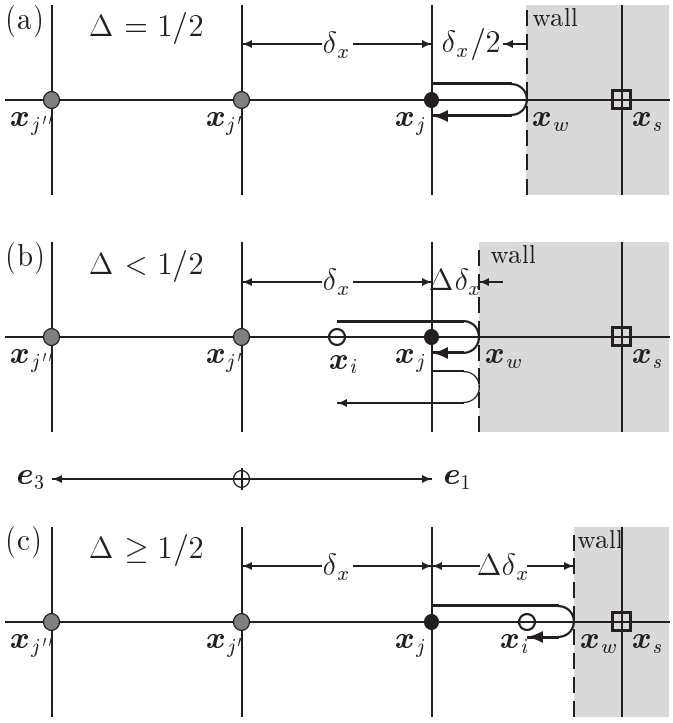

Figure 4.2: Illustration of the boundary conditions for a rigid wall located arbitrarily between two grid sites in one dimension. The thin solid lines are the grid lines, the dashed line is the boundary location situated arbitrarily between two grids. Shaded discs are the fluid nodes, and the discs (•) are the fluid nodes next to boundary. Circles (◦) are located in the fluid region but not on grid nodes. The square boxes (□) are within the non-fluid region. The thick arrows represent the trajectory of a particle interacting with the wall, described in Eqs. (4.3a) and (4.3b). The distribution functions at the locations indicated by discs are used to interpolate the distribution function at the location marked by the circles (◦). (a) $\Delta \equiv |\boldsymbol{x}_j - \boldsymbol{x}_w|/\delta_x = 1/2$. This is the perfect bounce-back scheme with no interpolations. (b) $\Delta < 1/2$. (c) $\Delta \geq 1/2$.

$\{f_\alpha\}$, the actual formulas used in simulations are:

$$f_{\bar{\alpha}}(\boldsymbol{x}_j, t) = \Delta\,(1+2\,\Delta) f_\alpha(\boldsymbol{x}_j + \boldsymbol{e}_\alpha \delta_t, t) + (1-4\,\Delta^2) f_\alpha(\boldsymbol{x}_j, t)$$
$$-\Delta\,(1-2\,\Delta) f_\alpha(\boldsymbol{x}_j - \boldsymbol{e}_\alpha \delta_t, t) + 3 w_\alpha (\boldsymbol{e}_\alpha \cdot \boldsymbol{u}_w)\,, \qquad \Delta < \frac{1}{2}, \quad (4.3a)$$

$$f_{\bar{\alpha}}(\boldsymbol{x}_j, t) = \frac{1}{\Delta\,(2\,\Delta+1)} f_\alpha(\boldsymbol{x}_j + \boldsymbol{e}_\alpha \delta_t, t) + \frac{(2\,\Delta-1)}{\Delta} f_{\bar{\alpha}}(\boldsymbol{x}_j - \boldsymbol{e}_\alpha \delta_t, t)$$
$$-\frac{(2\,\Delta-1)}{(2\,\Delta+1)} f_{\bar{\alpha}}(\boldsymbol{x}_j - 2\boldsymbol{e}_\alpha \delta_t, t) + \frac{3 w_\alpha}{\Delta\,(2\,\Delta+1)} (\boldsymbol{e}_\alpha \cdot \boldsymbol{u}_w)\,, \quad \Delta \geq \frac{1}{2}\,. \quad (4.3b)$$

The above formulas are implemented as follows. The collision-advection process

including the bounce-back collision with boundaries are divided in the following five steps:

- Step 1: Compute moments at all fluid nodes;
- Step 2: Relax the non-conserved moments at all fluid nodes, add momentum change if an external force is presented;
- Step 3: Compute the post-collision distributions $\{f_\alpha\}$ at all fluid nodes;
- Step 4: Advect $\{f_\alpha\}$ throughout the system, including all fluid and non-fluid nodes. Some distributions will be advected from fluid nodes to non-fluid nodes, and some from non-fluid nodes to fluid nodes.
- Step 5: Recompute the distributions that are advected from non-fluid nodes to fluid nodes according to Eq. (4.3a) or (4.3b), depending on the precise location of the boundary (*i.e.*, the value of Δ).

When boundaries lie in between two nodes of two grid points, the above implementation is equivalent to the so-called "node implementation" of the bounce-back scheme, *i.e.*, the bounce-back collision does not take time.

Two formulae (4.3a) and (4.3b) can be compressed to a single formula if the first-order interpolations are used [3, 63].

4.3 Applications

In the section we will mention concisely the areas in which the LBE method has been successfully applied, and provide some key references.

Flow through porous media. The key issue in the LBE direct numerical simulations (DNS) of flow through porous media is to accurately capture complicated boundary geometry even with very low resolutions. To this end, the lattice Boltzmann method has been successful [47, 61, 50]. This is due to the fact that the LBE method can accurately compute the mass/momentum transfers at boundaries [3, 49, 63].

Suspensions in fluids. The LBE method has been very successful in the direct numerical simulations of particulate and colloidal suspensions in fluids [34, 35, 51, 36, 52, 53, 54]. The LBE method has been effective in the simulations of a single particle in fluid [51, 52, 54] or the rheology of particulate suspensions [34, 35, 36, 53].

Mutli-component and interfacial dynamics. We mention in passing that the multicomponent LBE schemes can also be derived from the continuous Boltzmann equations for mixtures [44, 45]. The LBE method has applied to simulate interfacial phenomena (*e.g.*, [18, 6]).

Direct numerical simulations (DNS) of turbulence. Recent results show that the LBE method can reproduce well-known results for the homogeneous isotropic turbulence flow (*e.g.*, [46, 64]). And the LBE method can be vary competitive when compared with pseudo-spectral method.

Large eddy simulations (LES). The LBE-LES for turbulent flows is one of new areas. Most LBE-LES schemes use the Smagorinsky sub-grid model, which can be easily implemented in the LBE method [12, 11, 32, 33].

Non-Newtonian fluids. The LBE models for linear viscoelastic fluids have developed [19, 20, 38] and applied in simulations [18].

Epilogue

In five lectures I tried to give an overview on the theory of the lattice Boltzmann equation. The emphasis of these lectures is on the mathematical justification of the lattice Boltzmann method. Unfortunately I did not have the time to discuss the applications of the method, which I shall refer the readers to a recent review on the lattice gas and lattice Boltzmann method [43]. Here I would like to a few words on the rationale, or philosophy of the lattice gas and lattice Boltzmann methods.

It is a well known fact that a fluid is a discrete system with a large number ($\sim 10^{23}$) of particles (molecules). A system of many particles can be described by either molecular dynamics (MD) or a hierarchy of kinetic equations (the Bogoliubov-Born-Green-Kirkwood-Yvon hierarchy), and these two descriptions are equivalent. With the molecular chaos assumption due to Boltzmann, the BBGKY hierarchy can be closed with a single equation: the Boltzmann equation for the single particle distribution function. On the other hand, a fluid can also be treated as a continuum described by a set of partial differential equations for fluid density, velocity, and temperature: the Navier-Stokes equations. It should be stressed that the continuum treatment of fluid is an approximation. This approximation works extremely well under many circumstances.

It is usually convenient to use the Navier-Stokes equations to some fluid problems. Unfortunately these equations can be very difficult or even impossible to solve under some circumstances such as inhomogeneous multiphase or multicomponent flows, or granular flows. In the case of multiphase or multicomponent flows, interfaces between different fluid components (*e.g.* oil and water) or phases (*e.g.* vapor and water) cause the numerical difficulties. Computationally, one might be able to track a few, but hardly very many interfaces in a system. Realistic simulations of fluid systems with density or composition inhomogeneities by direct solution of the Navier-Stokes equations is therefore impractical. We can also look at the problem from a different perspective: interfaces between different components or phases of a fluid system are thermodynamic effects which result from interactions among molecules. To solve the Navier-Stokes equations, one needs to know the equation of state, which is usually unknown at an interface. It is therefore difficult to incorporate thermodynamics into the Navier-Stokes equations in a consistent or *a priori* fashion. Hence we encounter some fundamental difficulties. In the case of granular flow, the situation is even worse: it is not even clear that there exists a set partial differential equations analogous to the Navier-Stokes equations which correctly model such systems. Instead, granular flow is usually modeled by equations completely lacking

the fundamental validity of the Navier-Stokes equations.

Although the Navier-Stokes equations are inadequate in some circumstances, neither molecular dynamics nor the Boltzmann equation are practical alternatives because solutions of molecular dynamics or the Boltzmann equation pose formidable tasks which demand much more computational effort than the solution of the Navier-Stokes equations. Thus, we face the following predicament: although the Navier-Stokes equations are inadequate, molecular dynamics or the Boltzmann equation are much too difficult to solve and are even unnecessarily complicated if we are only interested in the macroscopic behaviors of a system. It is within this context that the lattice-gas automata (simplified molecular dynamics) and the lattice Boltzmann equation (simplified Boltzmann equation) become alternatives. It has been realized that hydrodynamics is insensitive to the details of the underlying microscopic or mesoscopic dynamics — the Navier-Stokes equations are merely statements of conservation laws, which reflect the same conservation laws in microscopic dynamics, and constitutive relations, which reflect the irreversible nature of the macroscopic dynamics. Different inter-molecular interactions would only result in different numerical values of the transport coefficients. Since the details of the microscopic dynamics are not important if only the hydrodynamic behavior of system is of interest, one may ask the following question: What constitutes a minimal microscopic or mesoscopic dynamic system which can provide desirable physics at the macroscopic level (hydrodynamics, thermodynamics, *etc.*). It turns out that the essential elements in such a microscopic or mesoscopic dynamic system are the conservation laws and associated symmetries. It is based upon this rationale that the lattice gas and the lattice Boltzmann models were constructed as reduced models to numerically simulate various complex systems.

It should also be pointed out that kinetic theory is valid for a wide range of densities covering gases, liquids, and even solids. It is within the framework and upon the foundation of kinetic theory that the lattice gas and lattice Boltzmann methods are formulated as consistent and effective simulation tools.

Since kinetic theory plays such an important role in the lattice gas and the lattice Boltzmann methods, it would be perhaps appropriate to end this series of lectures by quoting Professor E.G.D. Cohen [7] and Boltzmann [2] on their views on kinetic theory.

"*...I note that the objection is often raised that kinetic theory is restricted in its applications, is very complicated and that more general results can be much easier obtained by using hydrodynamic-like theories. All this is certainly true. However, if one is not just interested in obtaining new results, but also wants to understand their foundation in the molecular structure of matter and see the connection between various, at first sight, very different phenomena from a unified point of view, kinetic theory has proved to be an indispensable means to achieve this goal. In addition, it has led to new results, in spite of its complicated structure.*

"It seems to me then that kinetic theory finds itself at the end of the twentieth century again in an impasse and in a situation not too different from that in which it found itself at the end of the nineteenth century. It might therefore be appropriate to justify this survey by quoting some words Boltzmann used in 1898 ..."

E.G.D. Cohen (1993)

"*It was just at this time that attacks on the theory of gases began to increase. I am convinced that these attacks are merely based on a misunderstanding, and that the role of gas theory in science has not yet been played out. ...*

"In my opinion it would be a great tragedy for science if the theory of gases were temporarily thrown into oblivion because of a momentary hostile attitude toward it, as was for example the wave theory because of Newton's authority.

"I am conscious of being only an individual struggling weakly against the stream of time. But it still remains in my power to contribute in such a way that, when the theory of gases is again revived, not too much will have to be rediscovered. ... When consequently parts of the argument become somewhat complicated, I must of course plead that a precise presentation of these theories is not possible without a corresponding formal apparatus. ..."

L. Boltzmann (1898)

Reference

[1] Bhatnagar, P.L., Gross, E.P., and Krook, M. *A model for collision processes in gases. I. Small amplitude processes in charged and neutral one-component systems*. Phys. Rev. **94**:511–525 (1954).

[2] Boltzmann, L. *Lectures on Gas Theory*. (UC Press, Berkeley, 1964).

[3] Bouzidi, M., Firdaouss, M., and Lallemand, P. *Momentum transfer of a Boltzmann-lattice fluid with boundaries*. Phys. Fluids **13**:3452–3459 (2001).

[4] Chapman, S. and Cowling, T.G. *The Mathematical Theory of Non-Uniform Gases*. 3rd Edition, (Cambridge University Press, Cambridge, 1970).

[5] Chen, H., Chen, S., and Matthaeus, W.H. *Recovery of the Navier-Stokes equations using a lattice-gas Boltzmann method*. Phys. Rev. A **45**:R5339–R5342 (1992).

[6] Clark, T. *A numerical study of the statistics of a two-dimensional Rayleigh-Taylor mixing layer*. Phys. Fluids **15**:2413–2423 (2003).

[7] Cohen, E.G.D. *Fifty years of kinetic theory*. Physica A **194**:229–257 (1993).

[8] d'Humières, D. *Generalized lattice-Boltzmann equations*. in *Rarefied Gas Dynamics: Theory and Simulations*, Prog. Astronaut. Aeronaut. **159**:450–458, edited by Shizgal, B.D. and Weaver, D.P., (AIAA, Washington, D.C. 1992).

[9] d'Humières, D., Bouzidi, M., and Lallemand, P. *Thirteen-velocity three-dimensional lattice Boltzmann model*. Phys. Rev. E **63**:066702 (2001).

[10] d'Humières, D., Ginzburg, I., Krafczyk, M., Lallemand, P., and Luo, L.-S. *Multiple-relaxation-time lattice Boltzmann models in three-dimensions*. Philo. Trans. R. Soc. London A **360**:437–451 (2002).

[11] Derksen, J.J. and Van der Akker, H.E.A. *Simulation of vertex core precession in a reverse-flow cyclone*. AIChE J. **46**:1317–1331 (2000).

[12] Eggels, J.G.M. *Direct and large-eddy simulations of turbulenct fluid flow using the lattice-Boltzmann scheme*. Int. J. Heat Fluid Flow **17**:307–323 (1996).

[13] Filippova, O. and Hänel, D. *Grid refinement for lattice-BGK models*. J. Comput. Phys. **147**:219–228 (1998).

[14] Frisch, U., Hasslacher, B., and Pomeau, Y. *Lattice-gas automata for the Navier-Stokes equation*. Phys. Rev. Lett **56**:1505–1508 (1986).

[15] Frisch, U., d'Humières, D., Hasslacher, B., Lallemand, P., Pomeau, Y., and Rivet, J.-P. *Lattice gas hydrodynamics in two and three dimensions*. Complex Systems **1**:649–707 (1987).

[16] Ginzbourg, I. and Adler, P.M. *Boundary flow condition analysis for the three-dimensional lattice Boltzmann model*. J. Phys. II **4**:191–214 (1994).

[17] Ginzbourg, I. and d'Humières, D. *Local second-order boundary methods for lattice Boltzmann models*. J. Stat. Phys. **84**:927–971 (1996).

[18] Ginzburg, I. and Steiner, K. *A free-surface lattice Boltzmann method for modelling the filling of expanding cavities by Bingham fluids*. Philo. Trans. R. Soc. London A **360**:453–466 (2002).

[19] Giraud, L., d'Humières, D., and Lallemand, P. *A lattice-Boltzmann model for viscoelasticity*. Int. J. Mod. Phys. C **8**:805–815 (1997).

[20] Giraud, L., d'Humières, D., and Lallemand, P. *A lattice Boltzmann model for Jeffreys viscoelastic fluid*. Europhys. Lett. **42**:625–630 (1998).

[21] Grosfils, P. and Lallemand, P. *Dispersion effects in lattice gases with internal and translational mode-coupling*. Europhys. Lett. **24**:473–478 (1993).

[22] He, X. and Doolen, G. *Lattice Boltzmann method on a curvilinear coordinate system: Vortex shedding behind a circular-cylinder*. Phys. Rev. E **56**:434–440 (1997).

[23] He, X. and Doolen, G. *Lattice Boltzmann-method on curvilinear coordinates system: Flow around a circular-cylinder*. J. Comput. Phys. **134**:306–315 (1997).

[24] He, X. and Luo, L.-S. *A priori derivation of the lattice Boltzmann equation*. Phys. Rev. E **55**:R6333–R6336 (1997).

[25] He, X. and Luo, L.-S. *Theory of the lattice Boltzmann method: From the Boltzmann equation to the lattice Boltzmann equation*. Phys. Rev. E **56**:6811–6817 (1997).

[26] He, X. and Luo, L.-S. *Some progress in lattice Boltzmann method. 1. Nonuniform mesh grids*. J. Comput. Phys. **129**:357–363 (1996).

[27] He, X. and Luo, L.-S. *Some progress in the lattice Boltzmann method: Reynolds-number enhancement in simulations*. Physica A **239**:276–285 (1997).

[28] He, X., Shan, X., and Doolen, G.D. *Lattice Boltzmann simulation of non-ideal fluids*. Phys. Rev. E **57**:R13–R16 (1998).

[29] He, X., Zou, Q., Luo, L.-S., and Dembo, M. *Analytic solutions and analysis on non-slip boundary condition for the lattice Boltzmann BGK model*. J. Stat. Phys. **87**:115–136 (1997).

[30] Higuera, F.J. and Jiménez, J. *Boltzmann approach to lattice gas simulations*. Europhys. Lett. **9**:663–668 (1989).

[31] Higuera, F.J., Succi, S., and Benzi, R. *Lattice gas dynamics with enhanced collisions*. Europhys. Lett. **9**:345–349 (1989).

[32] Krafczyk, M. *Gitter-Boltzmann-methoden: von der theorie zuer anwandung*. Habilitation thesis, Technischen Universität Müchen (2001).

[33] Krafczyk, M., Tölke, J., Luo, L.-S. *Large-eddy simulations with a multiple-relaxation-time LBE model*. *Int. J. Mod. Phys. B* **17**, 33–39 (2003).

[34] Ladd, A.J.C. *Numerical simulations of particulate suspensions via a discretized Boltzmann equation. Part 1. Theoretical foundation*. J. Fluid Mech. **271**:285–309 (1994).

[35] Ladd, A.J.C. *Numerical simulations of particulate suspensions via a discretized Boltzmann equation. Part 2. Numerical results*. J. Fluid Mech. **271**:311–339 (1994).

[36] Ladd, A.J.C. and Verberg, R., *Lattice Boltzmann simulations of particle-fluid suspensions*. J. Stat. Phys. **104**:1191–1251 (2001).

[37] Lallemand, P. and Luo, L.-S. *Theory of the lattice Boltzmann method: Dispersion, dissipation, isotropy, Galilean invariance, and stability*. Phys. Rev. E **61**:6546–6562 (2000).

[38] Lallemand, P., d'Humières, D., Luo, L.-S., and Rubinstein, R. *Theory of the lattice Boltzmann method: Three-dimensional model for linear viscoelastic fluids*. Phys. Rev. E **61**:021203 (2003).

[39] Luo, L.-S., Chen, H., Chen, S., Doolen, G., and Lee, Y.-C. *Generalized hydrodynamic transport in lattice-gas automata*. Phys. Rev. A **43**:7097–7100 (1991).

[40] Luo, L.-S. *Analytic solutions of linearized lattice Boltzmann equation*. J. Stat. Phys. **88**:913–926 (1997).

[41] Luo, L.-S. *Unified Theory of lattice Boltzmann models for nonideal gases*. Phys. Rev. Lett. **81**:1618–1621 (1998).

[42] Luo, L.-S. *Theory of the lattice Boltzmann method: Lattice Boltzmann models for nonideal gases*. Phys. Rev. E **62**:4982–4996 (2000).

[43] Luo, L.-S. *The lattice-gas and lattice Boltzmann methods: Past, present, and future*. in Proceedings of Applied CFD 4, Beijing, October 16–19, 2000, pp. 52–83. (available at `http://research.nianet.org/~luo`.)

[44] Luo, L.-S., Girimaji, S.S. Lattice Boltzmann model for binary mixtures. Phys. Rev. E **66**:035301(R) (2002).

[45] Luo, L.-S. and Girimaji, S.S. Theory of the lattice Boltzmann method: Two-fluid model for binary mixtures. Phys. Rev. E **67**:036302 (2003).

[46] Luo, L.-S., Qi, D., and Wang, L.P. *Applications of the lattice Boltzmann method to complex and turbulent flows*. In *Lecture Notes in Computational Science and Engineering* **21**, edited by M. Breuer, F. Durst, and C. Zenger, pp. 123-130 (2002). (available at `http://research.nianet.org/~luo`.)

[47] Martys, N.S. and Chen, H. *Simulations of multicomponent fluids in complex three-dimensional geometries by the lattice Boltzmann method*. Phys. Rev. E **53**:743–750 (1996).

[48] McNamara, G. and Zanetti, G. *Use of the Boltzmann equation to simulate lattice-gas automata*. Phys. Rev. Lett. **61**:2332–2335 (1988).

[49] Mei, R., Yu, D., Shyy, W., and Luo, L.-S. *Force evaluation in the lattice Boltzmann method involving curved geometry*. Phys. Rev. E **65**:041203 (2002).

[50] Pan, C.X. *Use of pore-scale modeling to understand transport phenomena in porous media*. Ph.D. thesis, University of North Carolina at Chapel Hill, Chapel Hill, NC (2003). (available at `http://www.unc.edu/~dpan/`).

[51] Qi, D.W. *Lattice Boltzmann Simulations of particles in No-zero-Reynolds-number flows*. J. Fluid Mech. **385**:41–62 (1999).

[52] Qi, D.W., Luo, L.-S., Aravamuthan, R., and Strieder, W. *Lateral migration and orientation of elliptical particles in Poiseuille flows*. J. Stat. Phys. **107**:102–120 (2002).

[53] Qi, D.W., and Luo, L.-S. *Transitions in rotations of a nonspherical particle in a three-dimensional moderate Reynolds number Couette flow*. Phys. Fluids **14**(12):4440–4443 (2002).

[54] Qi, D.W., and Luo, L.-S. *Rotational and orientational behaviour of a three-dimensional spheroidal particles in Couette flow*. J. Fluid Mech. **477**:201–213 (2003).

[55] Qian, Y.H., d'Humières, D., and Lallemand, P. *Lattice BGK models for Navier-Stokes equation*. Europhys. Lett. **17**:479–484 (1992).

[56] Shan, X. and Chen, H. *Lattice Boltzmann model for simulating flows with multiple phases and components*. Phys. Rev. E **47**:1815–1819 (1993).

[57] Shan, X. and Chen, H. *Simulation of nonideal gases and liquid-gas phase-transitions by the lattice Boltzmann-equation*. Phys. Rev. E **49**:2941–2948 (1994).

[58] Swift, M.R., Orlandini, E., Osborn, W.R., and Yeomans, J.M. *Lattice Boltzmann simulations of liquid-gas and binary-fluid systems*. Phys. Rev. E **54**:5041–5052 (1996).

[59] Swift, M.R., Osborn, W.R., and Yeomans, J.M. *Lattice Boltzmann simulation of nonideal fluids*. Phys. Rev. Lett. **75**:830–833 (1995).

[60] Toffoli, T. and Margolus, N. *Cellular Automata Machines*. (MIT Press, Cambridge, 1987).

[61] Tölke, J., Krafczyk, M., Schulz, M., and Rank, E. *Lattice Boltzmann simulations of binary fluid flow through porous media*. Philo. Trans. R. Soc. London A **360**:535–545 (2002).

[62] Tölke, J., Krafczyk, M., Schulz, M., Rank, E., and Berrios, R. *Implicit discretization and nonuniform mesh refinement approaches for FD discretizations of LBGK models*. Int. J. Mod. Phys. C **9**:1143–1157 (1998).

[63] Yu, D., Mei, R., Luo, L.-S., and Shyy, W. *Viscous flow computations with the method of lattice Boltzmann equation*. Prog. Aerospace Sci. **39**:329–367 (2003).

[64] Yu, H., Girimaji, S.S., and Luo, L.-S. *Lattice Boltzmann simulations of decaying homogeneous isotropic turbulence with and without system rotation*. Submitted to Phys. Rev. E (2003).

[65] Wolfram, S. *Cellular automaton fluids 1: Basic theory*. J. Stat. Phys. **45**:471–526 (1986).